ABSTRACT

JUNE, MICHAEL SEAN. Static Efficiency of Positive and Negative Pin-Ring Type Electrohydrodynamic Air Moving Devices. (Under the direction of Dr. Kevin Lyons.)

As far back as 1709, under certain conditions, air flow was observed in the presence of high voltage. This phenomenon is an example of electrohydrodynamic flow. The presence of high voltage, on the order of thousands to tens of thousands of volts, along with one electrode of high curvature (sharp) and another electrode without sharp edges, will support an ionization cascade given an initial, natural ionization event. , Under the right conditions, this will result in a sufficient number of ions to move a measurable amount of air due to momentum transfer between the ions and the neutral gas molecules. The current study investigated the efficiency and air flow enhancements of a small, simple ionic air moving device that consisted of needles and a 25 mm diameter cylinder. It was found that there was an optimal cylinder length, needle distance, polarity, and voltage for both air flow and efficiency, and it was shown that increasing the number of needles, and therefore ionization sites increased air flow and efficiency. Most importantly, perhaps, was the discovery that the predominant academic literature measured and reported efficiency differently than industry, giving the impression that ionic air flow devices were far inferior in terms of efficiency to conventional fans and blowers. The current work has shown that application of industry standard techniques and methodologies has resulted in a more favorable comparison to conventional air moving devices, and has also revealed that the efficiency of ionic devices shows great sensitivity to the parameters investigated in this work.

Static Efficiency of Positive and Negative
Pin-Ring Type Electrohydrodynamic
Air Moving Devices

by
Michael Sean June

A dissertation submitted to the Graduate Faculty of
North Carolina State University
in partial fulfillment of the
requirements for the Degree of
Doctor of Philosophy

Mechanical Engineering

Raleigh, North Carolina

2010

APPROVED BY:

Dr. Kevin Lyons Committee Chair	Dr. Tiegang Fang
Dr. Alexi Saveliev	Dr. Thomas Ward

DEDICATION

For my wife, Tracy.

For my son, Nicholas.

For my son, Christopher.

For my daughter, Megan.

For my mother and father, Michael and Jennifer.

BIOGRAPHY

Michael Sean June was born in Westfield, New York and grew up in Richland, Washington. He attended the State University College at Fredonia, NY and earned a Bachelor's degree in Biology with a Minor in Music in 1989. He attended the Rochester Institute of Technology and earned both a Bachelor's and Master's Degree in Mechanical Engineering in 1999. Since graduation from RIT, he has worked for IBM as a Thermal Engineer.

ACKNOWLEDGEMENTS

I would like to thank Dr. Kevin Lyons for his support and guidance throughout this process. It simply would not have been possible to juggle work, family, and a higher education without such a patient and wise advisor.

Likewise, thanks to Drs Tiegang Fang, Alexi Saveliev and Thomas Ward for serving on my committee, and actively contributing to my success in this endeavor.

Thank you to James Kribs (NCSU) for his invaluable work, and thank you to Michael Purdy (IBM) for keeping me from experiencing 20,000 Volts first hand, and for his technical expertise.

Thanks to IBM for keeping me employed, funding my education, and providing laboratory space.

TABLE OF CONTENTS

LIST OF TABLES

LIST OF FIGURES

Chapter 1

Introduction

1.1 Scope of Work

The purpose of this work was to investigate the effect of various geometric parameters on the performance and efficiency of an ionic air moving device. During the course of this work, it was observed that the current academic literature was not following the same conventions on measuring, and reporting efficiency as the computer industry. The computer industry is a major consumer of air moving devices used to cool notebook computers, desktop workstations, rack mounted servers, and other similar devices. The methods used by the computer industry are therefore the methods used by the manufacturers of air moving devices. The result of this difference in approach between the researchers of ionic air moving devices and various industrial characterizations was that ionic air moving devices appeared to have much lower efficiency than conventional rotary devices. They have been, therefore, somewhat ignored by the computer industry for cooling applications.

1.2 Introduction to Ionic Air Moving Devices

As early as 1709 it was observed by Francis Hauksbee that when he got near certain devices with high voltage present, air flow was felt. The commonly told story is that he felt the air flow on his face upon coming very close to the high voltage device. Sir Isaac Newton (1718), Michael Faraday (1839) and James Clerk Maxwell (1873) observed and reported on the same phenomenon, but the first major study is attributed to Chattock in 1899. Chattock correlated air flow pressure to electrical current flowing between electrodes of specific geometry. Steutzer (1959) analyzed ionic flows using both gas and liquid as a working fluid, and Robinson (1961, 1962) is known for his comprehensive survey of prior work, and the history of ionic flows in addition to his own work on the subject. Perhaps some of the most comprehensive modern work on this subject was completed by Lawton and Weinberg in their investigation of combustion phenomena. The physics of the phenomena and defining equations are well defined in their book, *Electrical Aspects of Combustion* (1969).

The basic explanation of the phenomena is quite simple. Given a high strength electric field across two electrodes with specific geometries, air can be made to flow as ions formed as a result of the geometry and high electric field collide with surrounding neutral molecules, as they flow to the opposite electrode. Momentum transfer between the ions and the molecules results in a steady bulk air flow. A side effect of this process is ozone generation. There are also several other applications worth noting as follows.

1.3 Other Applications

Ionic devices have been successfully sold commercially as filtration devices. A common example is the Ionic Breeze tm, once sold by the Sharper Image. Various ionic air purifiers are still available, however their effectiveness in the home and the associated risks of ozone generation are subject to debate and in some cases litigation. Researchers however have found the technology to be effective in filtering soot from flames. Saxena *et al* (1982) surveyed the state of the art in particulate removal from high pressure, high temperature gasses using ionic filtration methods. Saito *et al* (1997, 1999) looked at soot emission from an acetylene diffusion flame in the presence of a high strength electric field. They reported on the effects on the flame shape as well. Sylvestre de Ferron *et al* (2008) reported reduction in soot particles from diesel exhaust using electrostatic filtration methods.

In addition to filtration of particulates in exhaust streams, researchers have been investigating how electric fields and ionic devices vary the combustion process in hopes of controlling combustion products. Thong and Weinberg (1971) looked at control of particulate suspensions, both liquid and solid, in the flame using electric fields. In addition to unwanted combustion products there are applications where the products of combustion are useful. Chakrabarty (2008) investigated separating combustion product particulates using electric fields, and similarly Zhao (2008) investigated particle agglomeration. The pharmaceutical industry is often mentioned as a potential user of this technology.

Many investigators have been looking at flame stabilization using either ionic air moving devices, which of course includes the high electric field, and also the electric field alone with the flame as the source of ions. In many cases this work has led to side investigations of ionic air moving devices. Carleton and Weinberg (1987) investigated simulating the effects of gravity on product convection using an electric field. The most prolific work recently has been completed by Dunn-Rankin along with Weinberg on several papers, *et al* (2002, 2003, 2005, 2006, 2006, 2007, 2008). Their work has covered many related topics such as use of the electric field to simulate gravity or conversely to counteract gravity (simulating microgravity), inducing swirl in the flame for stabilization, and optimization of ionic air moving devices. They have also numerically simulated the electric field and the resulting flow. Their geometric optimizations of the ionic air moving device were used as a starting point for the author's current work reported herein.

1.4 Ionic Air Moving Devices

Since Dunn-Rankin *et al*, there have been many researchers who have concentrated solely on ionic air moving devices. As of late, the most research has been by Jewell-Larsen and team (2004, 2006, 2008, 2009). Jewell-Larsen's work has led to practical devices which are currently marketed by Teserra Inc. The work involves numerical modeling leading to further optimizations, and most recently they have demonstrated a notebook computer completely cooled by ionic devices. Of interest in Jewell-Larsen's work as well as a major point in this work, is the efficiency of these devices. Moreau, Touchard, and Leger (2006, 2008) give an extensive derivation and historical review of the calculation of efficiency commonly used by the academic literature. They reference works by Goldman (1985) and Bondar (1986) wherein early work on efficiency characteristics was done. Kim, Park, Noh and Huang (2010) have recently investigated the efficiency of ionic air moving devices placed in series to increase the pressure generated, based on work by Rickard, Dunn-Rankin, and Weinberg (2006). Other notable work regarding flow characteristics and/or efficiency has been published by Komeili, Chang, and Harvel (2006), Komeili, Tsubone *et al* (2008, 2008), and Brown and Lai (2009). Takeuchi and Yasoka (2009) made a comparison of an ionic flow device to a similar sized axial fan, but the geometry of the ionic device is different than in the other studies referenced, and as will be discussed further, did not calculate efficiency in the same way as the manufacturer of the fan. They did, however use a consistent method for both the ionic device and the axial fan. Finally, the work has been extended to flow modification and aerodynamic effects by many researchers. Realizing, in some cases that the flow produced is not high enough to compete with conventional air moving devices in more extreme applications, Go, *et al* (2007) investigated using an ionic device to modify the boundary layer thus enhancing the cooling rather than driving the cooling. Yue *et al* (2006) did similar work. The literature shows overall that this is a promising technology with many potential applications. Recent advances by the above mentioned teams have brought these devices ever closer to practicality.

Chapter 2

Background

2.1 Mechanism of the Flow

The flow from an ionic air moving device is caused by momentum transfer between the ions and the neutral molecules in the working fluid. The breakdown of the working fluid into ions is due to the presence of a very high electric potential in the vicinity of an electrode with a very sharp curvature. The ions then flow due to the potential gradient. The working fluid could be air, as in an electrostatic air moving device or the working fluid may already be ionized as in the case of a flame. The common structure across ionic air moving devices is a thin electrode with a very sharp curvature, such as a small diameter wire or a needle often referred to as the “emitter”, and a larger blunt electrode, often referred to as the “collector”. This blunt electrode can be a flat plate, which is typically paired with a wire electrode (Figure 2.1), or a blunt ring electrode paired with a needle cathode (Figure 2.2). In some embodiments, the anode is a burner and the cathode is either a ring or a mesh over the flame.

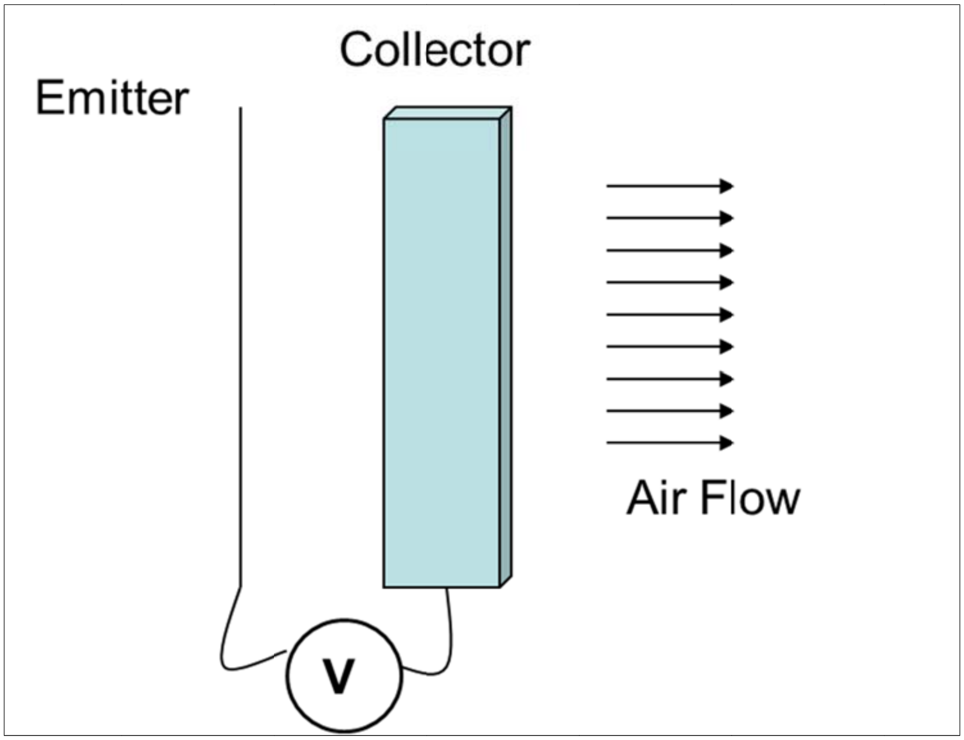

Figure 2.1 Schematic representation of wire and plate geometry for an ionic air moving device.

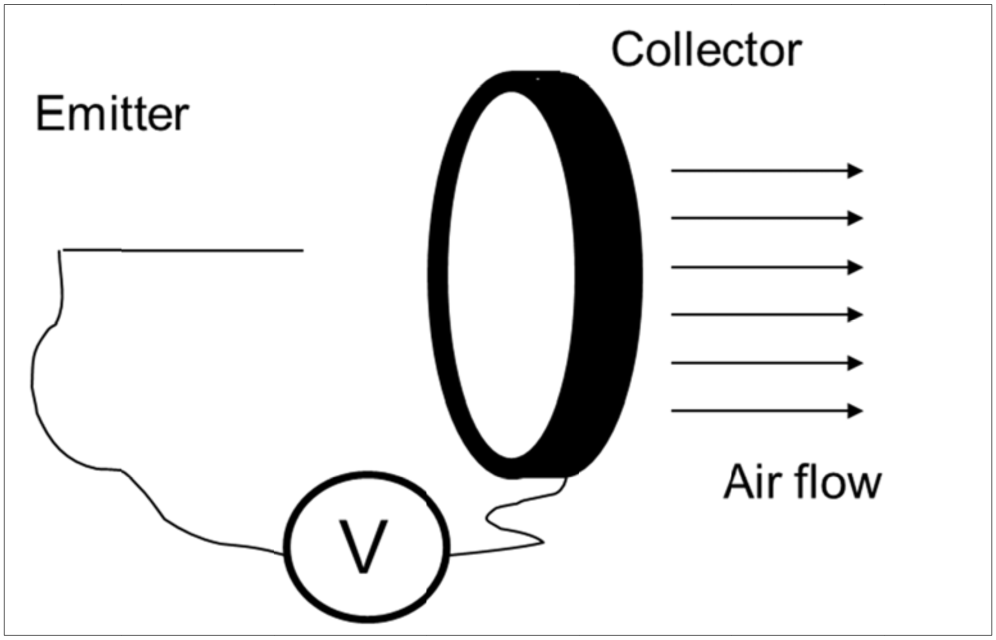

Figure 2.2 Schematic representation of needle and ring geometry for an ionic air moving device.

In an electrostatic field, the body force on a unit volume of the bulk gas is equal to the forces on the ions or other charged particles dispersed in the gas. This is provided that the ions or charged particles have constant mobility and do not accelerate. The force is given by

$$\overrightarrow{F} = \overrightarrow{E}e(n_{-} + n_{+}) \qquad 2.1$$

where $\overrightarrow{F}$ is the body force on a unit volume of air, $\overrightarrow{E}$ is the electric field, e is the fundamental charge, and n is the number density. Given the high electrical potential used to generate the ions and motivate the flow, it can be assumed that the clouds of ions are unipolar as long as secondary ionization is not occurring. Thus, the local current density,

$$\vec{j} = \overrightarrow{j_{+}} + \vec{j}_{-} = (K_{+}n_{+} + K_{-}n_{-})\overrightarrow{Ee}\,, \qquad 2.2$$

becomes

$$\vec{j} = (K_{\pm}n_{\pm})\overrightarrow{E}e \qquad 2.3$$

and

$$\overrightarrow{F_{\pm}} = \overrightarrow{E}e(n_{\pm})\,. \qquad 2.4$$

Combining, yields

$$\pm \vec{F} = \vec{j} / K_{\pm} \qquad 2.5$$

This equation describes the body force on a unit volume of air in terms of the local current density and the charge carrier mobility K.

The charged particles in the air stream can be generated as corona discharge from points of high curvature on an electrode given a sufficiently high potential. As the electric potential is increased beyond the point of ionization, the velocity of the air increases. It increases until secondary ionization occurs at the other electrode (Figure 2.3). Ions then begin to flow in the opposite direction, and therefore set up an opposing air flow. This necessitates large curvatures and polished surfaces on the "collector" electrode to delay the onset of the secondary ionization, and a sharp or small radius surface on the other "source" electrode to encourage primary ionization. This leads to the aforementioned pin/ring and wire/plate structures. If the electric potential is increased further, beyond the breakdown potential of the working fluid, arcing will occur (Figure 2.4). Ionic flows are also characterized by which electrode is positive and which is negative. If the source electrode is positive, it is characterized as a positive ionic flow, and conversely if it is negative, the flow is a negative ionic flow.

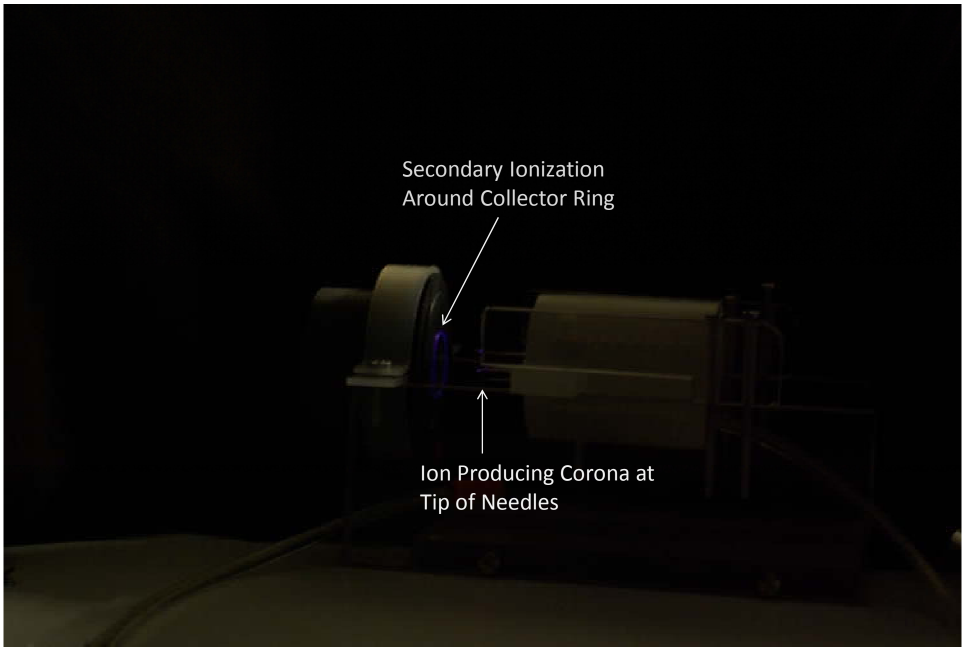

Figure 2.3 Photograph of the corona and secondary ionization on a needle and ring ionic air moving device.

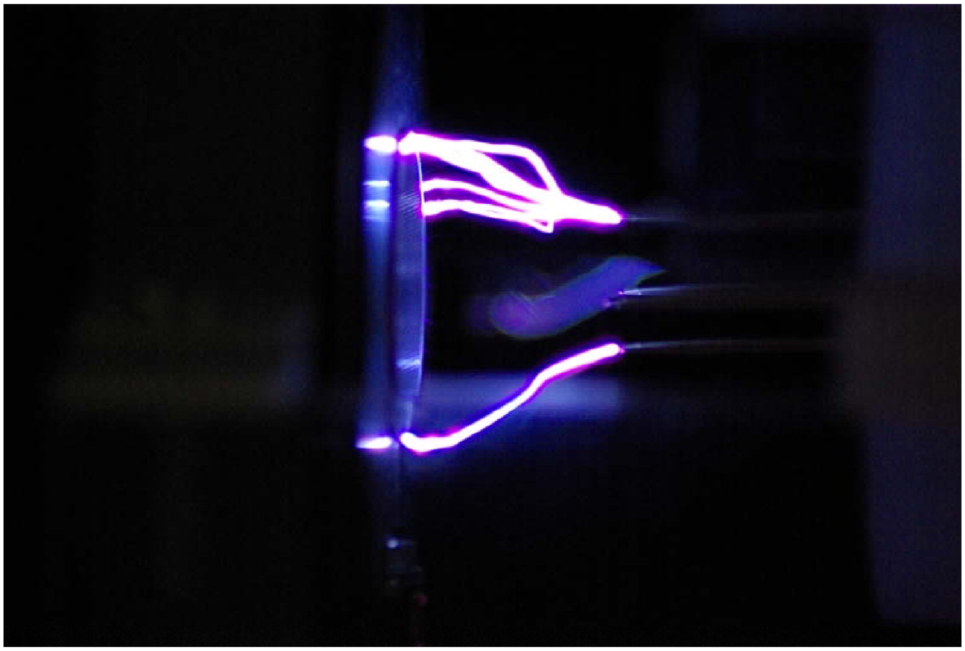

Figure 2.4 Photograph of arcing between needle and ring on an ionic air moving device.

2.2 Negative Corona

If the emitter electrode is on the negative side of the power supply, a “negative corona” will be generated given a high enough electric field. The mechanism and characteristics of the negative corona are significantly different than the “positive” corona which is generated when the emitter is on the positive side.

The negative corona consists of three concentric spheroid regions centered around the region of sharp curvature on the emitter electrode. These regions are the “Ionizing Plasma” region closest to the emitter, the “Non-Ionizing” region, and the “Unipolar” region farthest from the emitter. In the ionizing region, natural ionization events of the molecules of the working fluid occur due to interactions with photons, or from natural background radiation. Electrons along with the remaining positive species are created. If the electric field is sufficiently high, it prohibits the ion species from recombining. Peek’s Law (Peek, 1929) gives the voltage at which the onset of the corona occurs.

This is called the “Onset Voltage” or the “Corona Inception Voltage” and is given by

$$CIV = m_o E_o \delta (1 + .0301/(\delta r_w)^{\frac{1}{2}}) r_w \ln(d/r_w). \qquad 2.6$$

Where m_o is the wire roughness factor, typically 1 for polished metal, E_o is the working fluid breakdown field gradient at STP, typically $3e^6$ V/m for air, δ is the air density factor, typically 1 at STP, d is the distance between the electrodes, and r_w is the radius of the wire. Peeks Law is given in terms of a wire emitter, but can be used for a needle type emitter by iterating on the average thickness of the needle taper. Also due to the electric field, the electron moves toward the positive emitter and the positive ion moves toward the negative emitter (Figure 2.5).

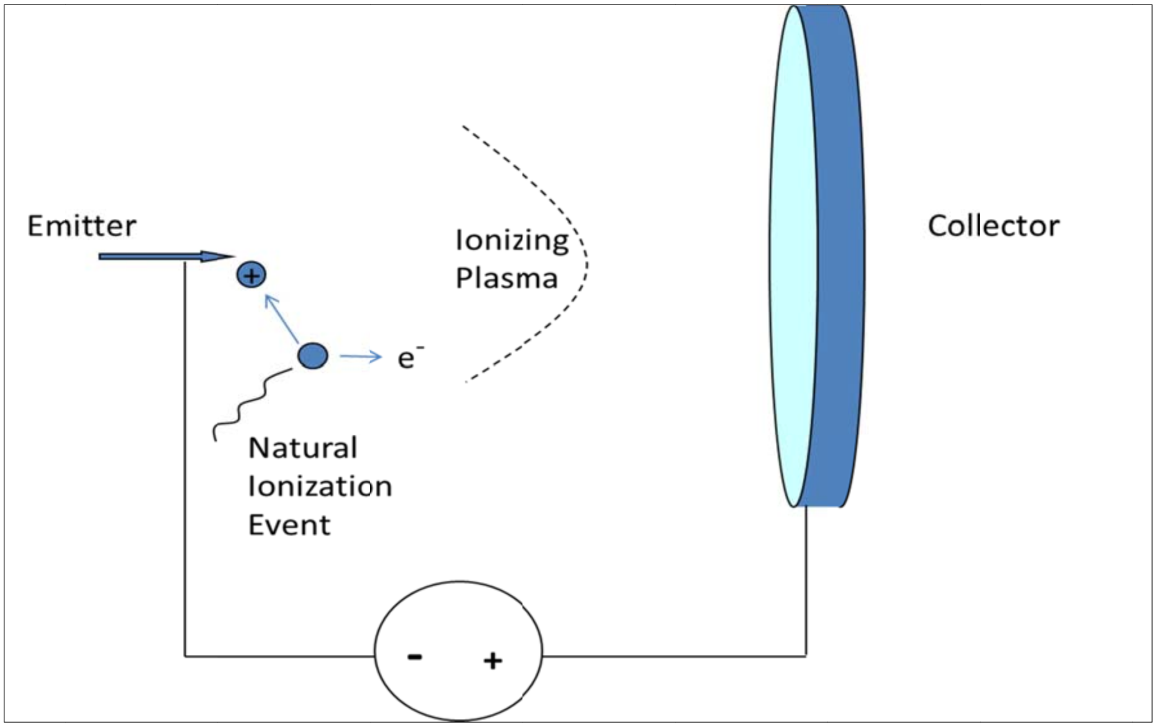

Figure 2.5 Beginning stages of the formation of a negative corona.

Natural ionization does not produce enough ions to sustain a corona. One key difference between positive and negative coronas is the way this natural ionization event leads to further ionization and a sustained corona. In the ionizing plasma region of the negative plasma, negative ions have sufficient energy to cause neutral molecules to ionize as a result of collision between the high energy ion and the neutral molecule. This results in a cascade of ions which sustain the corona. In addition to ionization of the neutral molecules in the working fluid, this process also occurs with molecules on the surface of the emitter electrode itself. As the electrons move away from the emitter, they lose energy until they no longer have enough to cause ionization upon collision with neutral molecules. Instead, they combine with the neutral molecules resulting in negatively charged molecules. This occurs in the non-ionizing plasma region. In the unipolar region there is no longer recombination taking place, rather momentum transfer between the neutral molecules and the negatively charged molecules mostly takes place in this region. Figure 2.6 shows a schematic overview of the negative corona and process.

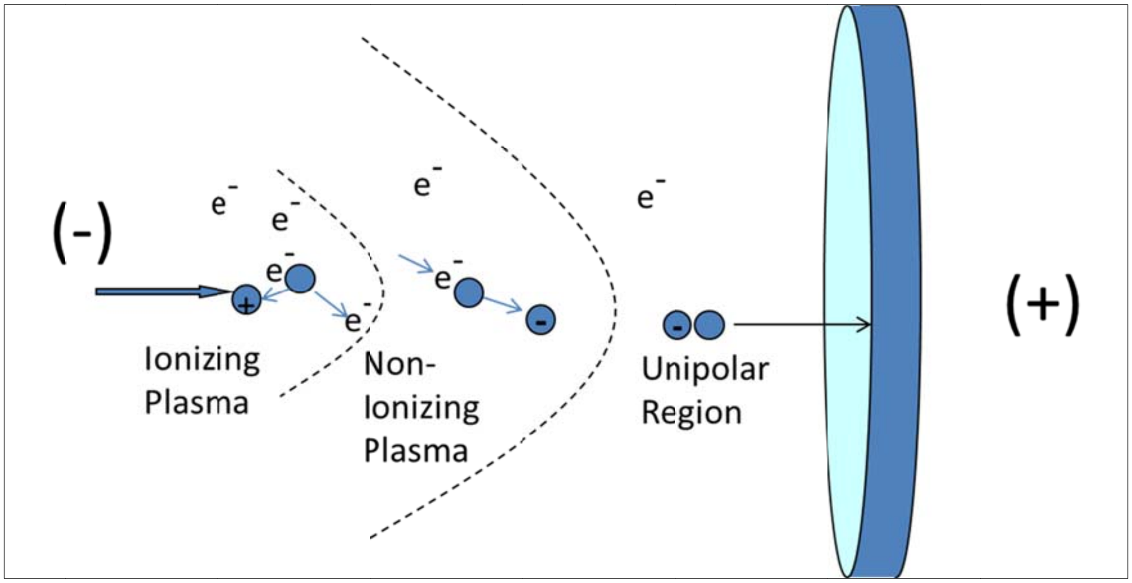

Figure 2.6 Three regions of a negative corona. Ionization occurs in the Ionizing Plasma region due to natural events, and due to cascading mechanisms. In the Non-Ionizing Plasma region, electrons lack sufficient energy for further ionization. Mostly recombination occurs. Mass transfer resulting in bulk flow occurs mainly in the Unipolar region.

Because electrons travel slower the further they get from the emitter, they tend to build up near the negative emitter. This locally reduces the electric field gradient and temporarily stops the ionization process. As the electrons drift away from the emitter, the local charge from the electrons dissipates, and the high electrical gradient is reestablished, thus starting the ionization process again. A characteristic of the negative corona, therefore is that it is pulsatile. This leads to emitted energy and electrical interference. While negative coronas are reported to have higher air flow than positive coronas (Chen and Davidson, 2003), these aforementioned characteristics along with increased ozone generation make the negative corona less suited for consumer applications.

2.3 Positive Corona

The positive corona consists of only two concentric spheroid regions centered around the region of sharp curvature on the emitter electrode. This is in contrast to the three regions of the negative corona. These regions are the “Ionizing Plasma” region closest to the emitter, and the “Unipolar” region farthest from the emitter. Once again, the process is initiated by a natural ionization event in the vicinity of the emitter, and if according to Peek’s Law the voltage is high enough, the species will remain separated and move towards the opposite electrodes. In this case, the electrons move toward the emitter which is closer, and more have enough energy to cause an ionization cascade. The positive ions drift directly into the Unipolar region and the working fluid flows due to momentum transfer between the positive ions and the neutral molecules of the working fluid. The momentum transfer in both the positive and the negative ionic flow is assumed to be without losses (Weinberg, 1969). The positive corona is not pulsatile, generates less ozone, and is better suited to consumer applications. Since it is not pulsatile, electrical interference is lower and it is, therefore better suited to cooling interference sensitive applications such as computers. Figure 2.7 shows a schematic representation of the positive corona.

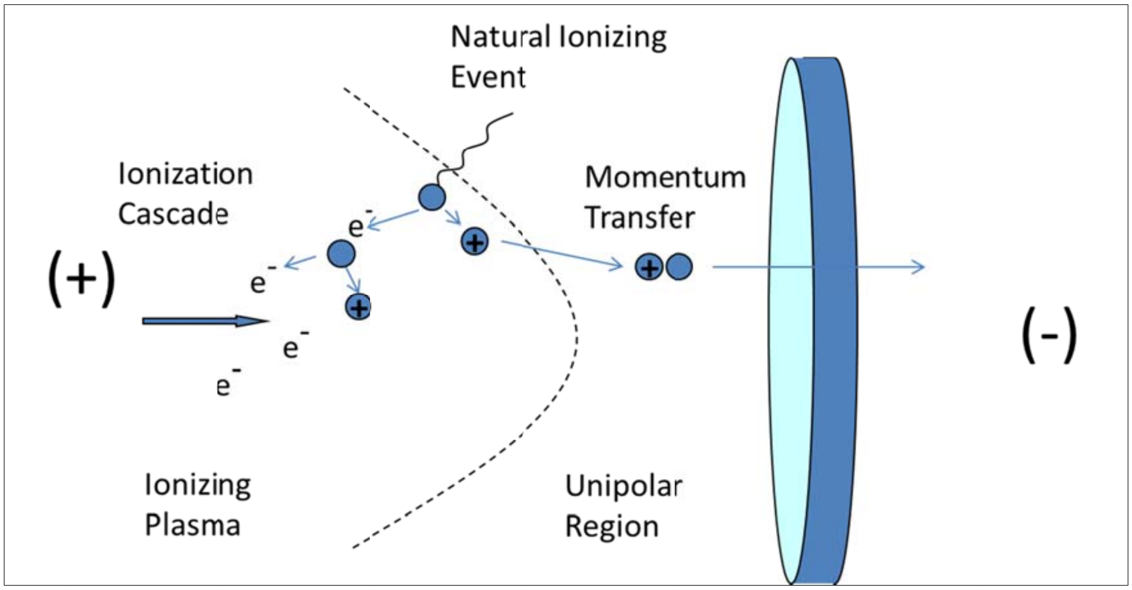

Figure 2.7 Two regions of a Positive corona. Ionization occurs in the Ionizing Plasma region due to natural events, and due to cascading mechanisms. Mass transfer resulting in bulk flow occurs mainly in the Unipolar region.

2.4 Efficiency

The efficiency of ionic air moving devices (AMDs) is discussed in several papers (Rickard, 2006, Moreau, 2008, Kim, 2010, Bondar, 1986, Goldman, 1985), however these calculations of efficiency and methodology of determining efficiency vary from what is used by the computer industry. That industry as well as companies that supply rotary AMDs to it, follow a method outlined by the ASME in ASME PTC 11-2008 (2008). A similar method is outlined by ASHRAE and ANSI as ANSI/ASHRAE 51-1999 (1999). The approach followed by academic literature regarding ionic AMDs results in lower reported efficiency for the ionic devices than would be reported if the industry preferred method was used. One goal of this paper is to explain the differences, and applicability of these methods and to evaluate the efficiency of ionic AMDs using the ASME/ANSI/ASHRAE methodology.

There is agreement that efficiency is defined as power supplied by the AMD divided by the electrical power supplied to the AMD

$$\eta = \frac{P_{out}}{P_{in}}, \text{ or } \eta = \frac{P_{mech}}{P_{electrical}} \tag{2.7}$$

but the discrepancy is in how the power supplied by the AMD is defined. Moreau (2006) provided a detailed derivation typical of the academic literature, starting from conservation of kinetic energy inside a control volume, and obtained

$$P_{mech} = \frac{1}{2}\rho\pi\int_{-D/2}^{+D/2} U^3(y)\left|y\right|dy \qquad (2.8)$$

where ρ is the density of the ambient air, and U^3 is the cubed velocity profile of the air. A circular collector was assumed, so this was essentially a cubed linear velocity, multiplied by area and again multiplied by density. Much of the literature follows a similar approach. Moreau's derivation began with the further assumption that linear velocity would be measured at various points to obtain a flow profile. This was integrated as a function to obtain the flow rate.

$$Q = \iint_S U(y,\theta)dS = \iint_S U(y,\theta)ydyd\theta \qquad (2.9)$$

Assuming axial symmetry, Q becomes

$$Q = \int_0^{2\pi} d\theta \times \int_0^{+D/2} U(y)dy = 2\pi \times \int_0^{+D/2} U(y)dy = \pi \times \int_{-D/2}^{+D/2} U(y)\left|y\right|dy \qquad (2.10)$$

Moreau (2007)

Starting from Conservation of kinetic energy inside a control volume, Moreau generally defines mechanical power.

$$\rho \frac{d}{dt}\left(\frac{1}{2}v^2\right) = -\vec{v}\cdot\vec{\nabla}P + \rho\vec{g}\cdot\vec{v} + \vec{v}\cdot\left(\vec{\nabla}\cdot\vec{\tau}\right) = T \tag{2.11}$$

The time rate of change of kinetic energy per unit volume is on the left and the terms on the right, from left to right are as follows: rate of work done by pressure forces per unit volume per unit time, rate of work performed by body forces per unit volume per unit time, and rate of work done by viscous forces per unit volume per unit time.

Because the following is true,

$$\rho \frac{d}{dt}\left(\frac{1}{2}v^2\right) = \frac{\partial}{\partial t}\left(\frac{1}{2}\rho v^2\right) + \vec{\nabla}\cdot\left(\frac{1}{2}\rho v^2\vec{v}\right) \tag{2.12}$$

Moreau integrated over a volume assuming the stationary case,

$$\int_V \vec{\nabla}\cdot\left(\frac{1}{2}\rho v^2\vec{v}\right)dV = \int_V T dv \tag{2.13}$$

and applied the Green-Ostrogradsky theorem to obtain

$$\int_V \vec{\nabla} \cdot \left(\frac{1}{2} \rho v^2 \vec{v} \right) dV = \int_S \frac{1}{2} \rho v^2 \vec{v} \cdot \vec{n} dA \qquad (2.14)$$

and finally,

$$\int_S \frac{1}{2} \rho v^2 \vec{v} \cdot \vec{n} dA = \int_V T dV \qquad (2.15)$$

(Moreau 2006)

For the case of an ionic air moving device with a circular cross section, this becomes equation 2.8.

$$P_{mech} = \frac{1}{2} \rho \pi \int_{-D/2}^{+D/2} U^3(y) |y| dy \qquad (2.8)$$

Moreau (2007) states also that mechanical power of an air flow in a duct is given by

$$P_{mech} = \frac{1}{2} \rho V^3 \qquad (2.16)$$

It is easy to see the similarity between equations 2.8 and 2.16. The difference is due to the integration of the velocity profile over the area.

Kim et al (2010) similarly defined mechanical power as

$$P_{mech} = \frac{1}{2}\dot{m}U^2 \tag{2.17}$$

Jewell-Larsen (2006) used a “pump efficiency” metric which was volumetric air flow divided by electrical power with the resulting units [cm^3/sW].

These approaches, however mathematically defensible, do not account for how efficiency changes when the air moving device is under load. In other words, the approach taken by the literature is only valid for an air moving device in open air, but not one that is working against the flow impedance provided by a heat sink , for example. In these cases efficiency is often plotted against flow rate or voltage as the independent variable. In the next example and in the methodology followed in this work, static pressure is varied while the electrical input to the device is held nearly constant.

Two methods for determining fan efficiency, defined in ASME PTC 11-2008 allow measurement of fan efficiency with static or total pressure, ie load as the independent variable. Once again, these methods are common to the computer industry, and the fan vendors which supply that industry. One of these methods has been used by the authors in previous research (June *et al*, 2010) and is the method followed in the current work. Derivations of these methods are shown in a paper by Kroll (1982). The first method considered is to multiply the volumetric flow rate by a quantity known as the fan specific energy which is energy per unit mass, given by

$$y_f = \frac{P_{s2} - P_{s1}}{\rho_m} + \frac{\dot{m}_F^2}{2g_c}\left[\frac{\alpha_2}{\rho_2^2 A_2^2} - \frac{\alpha_1}{\rho_1^2 A_1^2}\right] \tag{2.18}$$

where P_{s2} is the static pressure down stream from the fan, P_{s1} is the static pressure up stream from the fan, ρ_m is the mean density of the working fluid, $\dot{m}$ is the mass flow rate of the working fluid, g_c is acceleration due to gravity, α_1 and α_2 are kinetic energy conversion factors up stream and down stream, ρ_1 and ρ_2 are up stream and down stream local densities, and A is the cross sectional area of the duct up stream and down stream.

The other method, used most often by the computer industry, and by the authors in this study, takes the volumetric flow rate and multiplies it by static pressure or alternatively by total pressure. Total Efficiency which is defined as

$$\eta_t = \frac{QP}{VI}_t \tag{2.19}$$

where Q is the volumetric flow rate in m^3/s and P_t =Total Pressure. V is the voltage supplied to the air moving device, and I is the current drawn by the device. From this, Static Efficiency is defined as

$$\eta_s = \eta_t \frac{P_s}{P_t} \tag{2.20}$$

which reduces to

$$\eta_s = \frac{QP_s}{VI} \tag{2.21}$$

Kroll's derivation starts with the General Energy Equation from the First Law of Thermodynamics

$$\wp - \dot{Q} = \dot{m}_2\left(u_2 + \frac{P_2}{\rho_2} + e_{k_2} + e_{p_2}\right) - \dot{m}_1\left(u_1 + \frac{P_1}{\rho_1} + e_{k_1} + e_{p_1}\right) \tag{2.22}$$

where $\wp$ is the fan input power, $\dot{Q}$ is the heat loss from the fan, $\dot{m}_2$ is the mass flow rate, u is the internal energy, P is pressure, ρ is density, e_k is kinetic energy per unit mass, and e_p is the potential energy per unit mass.

Ignoring changes in potential energy and heat loss (customary in fan engineering per Kroll), equation 2.22 becomes,

$$\wp = \dot{m}_2 \left[C_v \left(T_2 - T_1 \right) + \frac{P_2}{\rho_2} - \frac{P_1}{\rho_1} + e_{k_1} - e_{p_1} \right] \qquad (2.23)$$

Kroll then invokes the Mechanical Energy, or “Generalized Bernoulli” Equation from Newton’s second law of mechanics ,

$$\wp - \wp_F = \iiint (\vec{V} \bullet \vec{\nabla} p) d\cancel{V} + \dot{m} \left[\left(e_{k_2} - e_{k_1} \right) + \left(e_{p_2} - e_{p_1} \right) \right] \qquad (2.24)$$

where $\wp_F$ is the friction power and $\cancel{V}$ is volume.

By considering flows along streamlines through the fan, and ignoring changes in potential energy, equation 2.24 is reduced to,

$$\wp - \wp_F = \dot{m} \left[\int_1^2 \frac{dp}{\rho} + e_{k_2} - e_{k_1} \right] \qquad (2.25)$$

If the process is considered to be incompressible, then equation 2.25 can be subtracted from equation 2.22 resulting in,

$$\wp_F - \dot{Q} = C_v(T_2 - T_1) \qquad (2.26)$$

For incompressible flows,

$$\rho Q = \dot{m} \qquad (2.27)$$

Therefore, equation 2.25 becomes,

$$\wp - \wp_F = Q\left[\left(p_2 + \rho e_{k_2}\right) - \left(p_1 + \rho e_{k_1}\right)\right] \qquad (2.28)$$

or

$$\wp - \wp_F = Q\left[p_{f\,2} - p_{f\,1}\right] \qquad (2.29)$$

Equation 2.29 is known as the fan output power equation, where p_f is the fan pressure rise.

To get to the form of the equation used most commonly by the computer industry and its fan vendors, one must consider that the previous equations are the basis for the definitions of flow rate, ideal energy rise, and fan output power. These are the performance variables that need to defined in order to determine a useful metric for fan efficiency, and thus for the efficiency of the ionic devices under consideration.

In what Kroll defines as the "Volume Flow Rate – Pressure Approach to Defining Fan Performance Variables," volume flow rate, and fan total pressure are chosen as primary performance variables. This is considering fan total pressure to be a type of energy per unit volume.

The fan total Pressure is,

$$p_{ft} = (p_2 + \rho_2 e_{k_2}) - (p_1 + \rho_1 e_{k_1}) \tag{2.30}$$

Density may change between the inlet and the outlet of the fan, so density, in this method, is taken at the inlet, so the volumetric flow rate is considered to be,

$$Q_f = \frac{\dot{m}}{\rho_{f_1}} \tag{2.31}$$

For incompressible flow, fan power simply becomes,

$$\wp_O = p_{ft} Q_f \tag{2.32}$$

which is the fan total pressure and the volumetric flow rate.

If the flow is compressible, a compressibility coefficient, K_p is factored in,

$$\wp_O \equiv \dot{m}\left[\int_1^2 \frac{dp}{\rho} + e_{k_2} - e_{k_1}\right] \cong K_p Q_f p_{ft} \tag{2.33}$$

Kroll references ASHRAE 51-75 (1975) for further explanation and development of K_p, however due to the low speeds involved in the current work, compressibility was not considered. It is presented here for completeness.

Kroll defines "fan total efficiency" as

$$\eta_t = \frac{\wp_O}{\wp} = \frac{K_p Q_f p_{ft}}{\wp} \tag{2.34}$$

Static pressure, which is considered in the current work, is further defined as,

$$P_{fs} = P_2 - (p_1 + \rho_1 e_k) \qquad (2.35)$$

which is the difference between outlet static pressure and inlet total pressure. Static pressure in general is a property “obtained in an isentropic-workless deceleration from the actual fluid state to a state with zero velocity” (Kroll, 1982). Simply stated, while dynamic pressure is measured with a tube aligned with the air flow, and is the pressure due to the flow itself, static pressure is measured with a tube perpendicular to the flow. This is typically measured as gage pressure and is only non-zero when the flow is restricted, and thus pushing against said restriction. Static efficiency is then defined as,

$$\eta_s = \eta_t \frac{p_{fs}}{p_{ft}} \qquad (2.36)$$

This is equivalent to,

$$\eta_s = \frac{Q_f\, p_{fs}}{\wp} = \frac{Q_f\, p_{fs}}{VI} \qquad (2.37)$$

This is the preferred metric since static pressure and volumetric flow rate are the independent and dependent variables respectively, of a fan performance curve. The data for both the fan performance curve and the static efficiency curve are collected concurrently.

These methods utilize an apparatus commonly referred to as an Air Flow Bench which is generally described in ANSI/ASHRAE 51-1999 (1999). The air flow bench used in the current study is described in greater detail in the following section, but is essentially a device for determining the air flow produced by an AMD at a constant voltage (or speed setting in the case of a fan or blower) as back pressure is varied from zero (open, or maximum flow) to the maximum pressure that the AMD can generate (completely restricted flow). This data is used to generate a fan performance curve which is typically overlaid on an impedance curve of whatever system the AMD is intended to operate in, thus determining the operating point of the device (Fox, 1992). As mentioned previously, this data, along with input power to the fan, is also used to generate an efficiency curve which will show the peak efficiency of the device along with the efficiency at the operating point as a function of volumetric air flow. Figure 2.8 shows a typical fan performance curve along with a static efficiency curve for a typical axial fan.

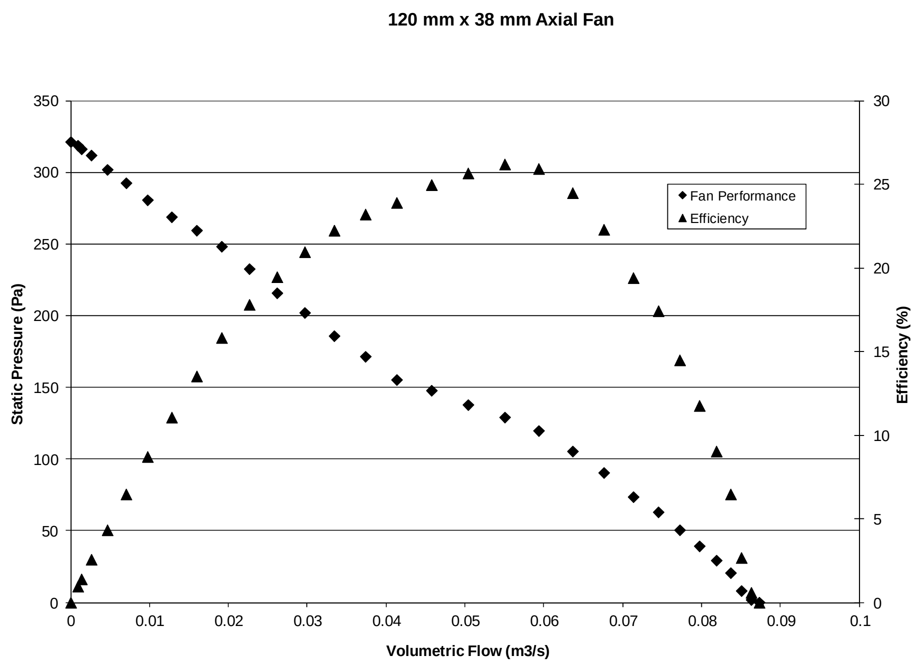

Figure 2.8 Typical fan performance and efficiency curves.

If it is necessary to determine the efficiency at various fan speeds, or in the case of ionic AMDs, supplied voltages, then it is necessary to generate these fan curves and efficiency curves at various voltages Then from each curve either the peak efficiency would be taken and plotted against voltage, or the efficiency at some intended operating point may be of more interest and this plotted against voltage.

The methodology used by the academic literature regarding ionic AMDs will agree with the latter at the point of open, unrestricted flow if Total Efficiency (η_t) is being evaluated. This is a very small value, typically, as compared to the peak efficiency. Since conventional fans and blowers are evaluated using the ASME methodology while the literature has predominantly evaluated efficiency with a different method, values much lower than peak have been reported. This makes ionic AMDs appear much less efficient than fans and blowers, since the literature doesn't clearly outline the differences in nomenclature or methodology.

2.5 Air Flow Bench

Air flow rate and static pressure were measured using a typical air flow bench (Figure 2.9). An air flow bench consists of an air flow source, in this case a centrifugal blower, to evacuate air from a Lexan chamber. Located between the blower and the chamber is a ball valve to regulate air flow, and typically a calibrated orifice of some type to measure volumetric air flow leaving the chamber was also utilized. Additionally there is a pressure sensor to detect the static pressure in the chamber relative to atmospheric pressure The device being tested is configured to blow into the chamber. Initially the air flow out of the chamber is adjusted until there is a reading of zero static pressure. At this point it is assumed that the air flow out of the chamber is equal to the flow into the chamber and thus the open flow rate of the device is determined. The valve is then closed in increments to simulate various loads on the AMD. At each point static pressure and air flow are determined. This is continued until the valve is fully closed. This is the point of maximum static pressure and zero air flow. At each point the voltage and current supplied to the AMD is recorded, and static efficiency is determined from these data.

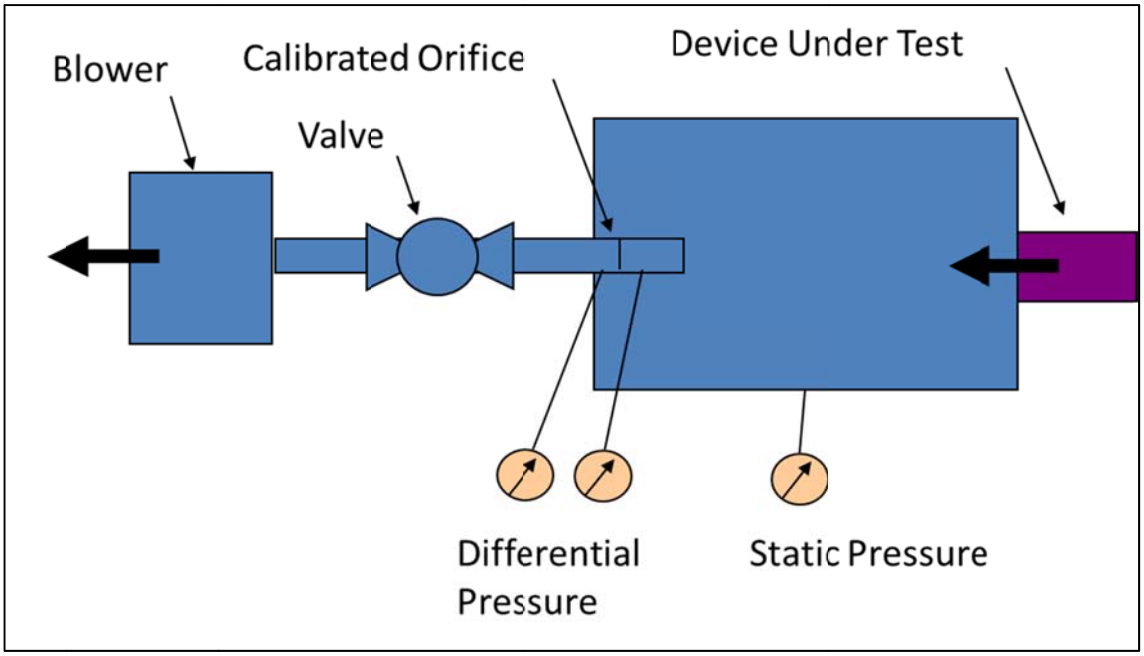

Figure 2.9 Schematic representation of typical air flow bench.

Chapter 3

Experiments

3.1 Overview

A flow bench and ionic air moving device were constructed to investigate the flow and efficiency characteristics of a needle and ring-type ionic flow device. In total the apparatus consisted of several volt meters, various manometers, and linear flow elements to measure volumetric flow rate, in addition to the actual air moving device. The experiments were performed at IBM's facilities in Research Triangle Park, North Carolina with much of the equipment provided by IBM. Therefore, much of the equipment used was calibrated by a third party to NIST traceable standards. The ionic flow device was fabricated at North Carolina State University with some modifications made by various model shops within IBM. The needles used as emitters were common size 22 sewing needles with the eyes cut off to a common length to fit in the needle holder. The needles were stated by the manufacturer to be nickel plated steel. The emitter cylinders were constructed of aluminum tubing (25.4 mm ID, 26.6 mm OD) cut to various lengths. The cylinders were sanded and polished to eliminate burrs and rough edges, then polished to a reasonable surface finish. The goal was to achieve a consistent surface finish such that it wasn’t a variable in the experiments, but such that it was an achievable, cost effective surface finish in terms of quality and variability. Given that the ultimate goal was to evaluate the feasibility of using ionic air moving devices to cool electronic equipment in place of conventional fans, they needed to be representative of what would be achievable at a comparative cost to the fans. This meant highly polished surfaces on the emitter needed to be avoided. Plating was acceptable on the needles since they are a high volume, common item, however in reality a purpose built emitter array for a production ionic air moving device would likely not have plated emitter needles.

Experiments were performed in a climate controlled laboratory, with little variation in ambient temperature and humidity within each dataset. Humidity has been identified in the literature to have an observable effect on air flow. It was not observed to have an effect within the variation in the laboratory where the experiments were performed.

The following sections are excerpts from three papers submitted for review or published by either the Journal of Electrostatics (Elsevier) or the Journal of Thermal Science and Engineering Applications (ASME). The introduction sections of each paper have been removed as the material has been covered in aggregate in previous sections of this work.

The papers cover the following experiments and results.

1) The effect on air flow and efficiency of varying the distance between the needle emitters and the cylindrical collector. This was performed with various collector lengths.

2) The effect on efficiency of varying voltage for a fixed ring length and needle distance. The ring length and needle distance chosen were the most efficient as observed in previous experiments.

3) The effect on air flow and efficiency as the number of emitter needles was varied.

4) The effect on air flow and efficiency as the ring thickness was varied as maximum air flow was held constant.

5) The effect on air flow and efficiency as the number of emitter needles was varied as maximum air flow was held constant.

6) The effect on efficiency as voltage was varied. This was performed with both a positive and a negative ionic flow.

7) The effect on efficiency as collector length was varied for both positive and negative ionic flow.

8) Comparison of a similar sized fan/heat sink combination to an ionic device using a heat sink as a collector.

Chapter 4

Excerpts from:

M.S. June, J. Kribs, K.M. Lyons, Efficiency of Electrostatic Air Moving Devices, J. Electrostat, 68 (2010) 419-423

4.1Procedure

An ionic air moving device was constructed using various aluminum rings, all 25.4 mm inside diameter and of various widths for the collector, along with up to 5 x 1.3 mm diameter sewing needles as the emitters. A cylindrical plastic fixture was fabricated to hold the rings, and to affix a ground wire to the ring. The needles were held in one of three cylindrical aluminum fixtures. One such fixture held 3 needles, one held 2 or 4, and the other held 5. These fixtures held the needles on a 12.2 mm diameter circle. Figure 4.1 shows a side view of the apparatus attached to a flow bench. Figure 4.2 shows the needle holder rotated away from the ring.

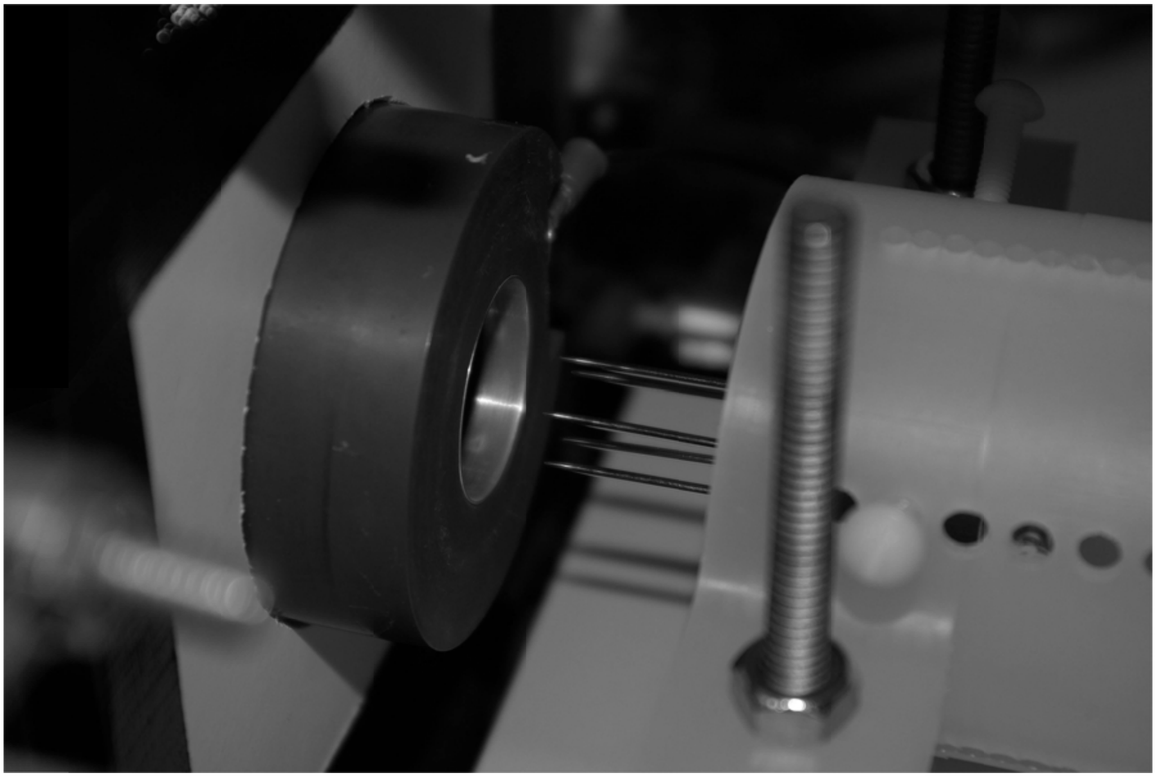

Figure 4.1 Photograph of experimental apparatus showing the ring electrode and 5 needle electrodes.

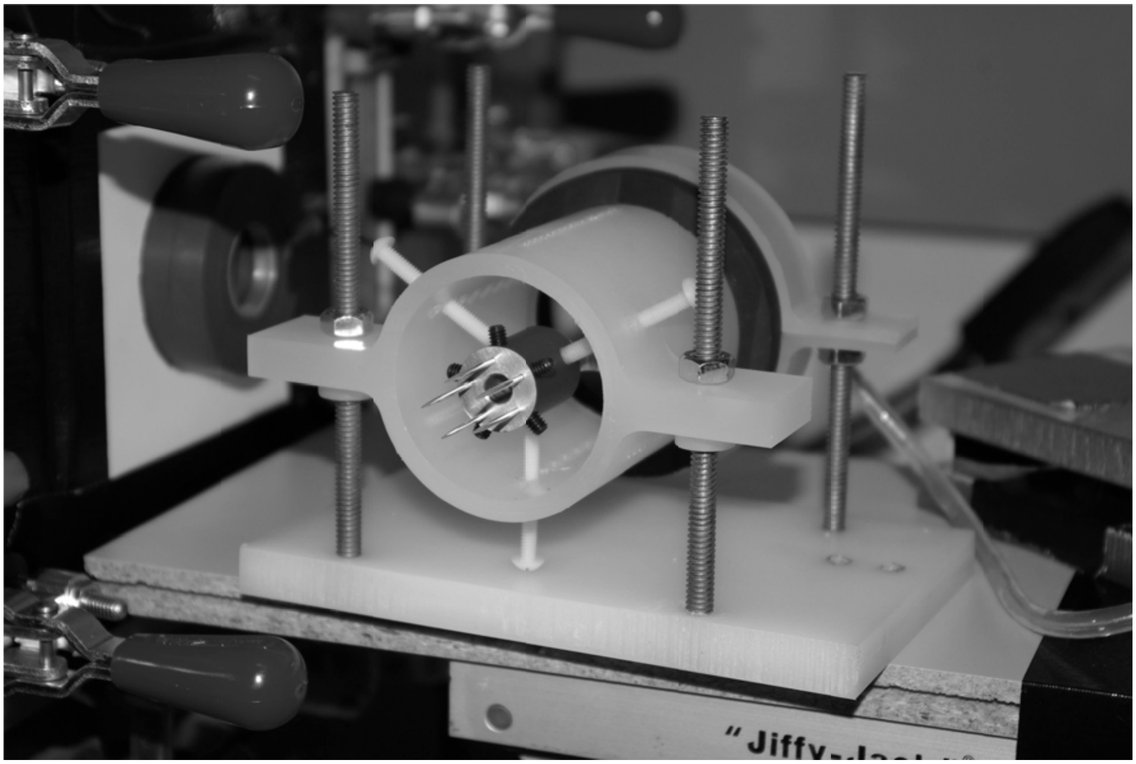

Figure 4.2 Photograph of experimental apparatus with the needle electrodes rotated 90-degrees to show the arrangement of the needles.

A 20kV Acopian DC power supply was used to supply a potential between the needle and the aluminum ring. A negative potential was applied to the needle, and the aluminum ring was grounded.

Air flow and back pressure were measured with a flow bench using a Meriam model 50MC2-2F linear flow element and a Meriam model LFS-1180E-99SP-5-31-1-99 to read air flow, and ambient conditions. Static pressure was measured with an MKS model 698A11TRD differential manometer.

Voltage was measured using a Hewlett Packard HP3466A DMM attached to the voltage sense terminals of the Acopian power supply. Current was measured also using a Hewlett Packard HP3466A DMM attached to the current sense terminals on the Acopian power supply. The offset for voltage readings was 1 V indicated for 10,000 V output. For the current measurement, 1 V indicated 1 mA output.

Pressure (P) was varied and the corresponding volumetric flow (Q) was measured on the flow bench to generate a P-Q curve. The air flow was initially balanced such that the flow bench blower was moving the same amount of air as the ionic device. At this point, there was no difference in pressure between the outlet of the ionic device, and the atmosphere. This was the point of maximum flow. A valve between the flow bench blower and the ionic device was then closed incrementally, thus varying the back pressure on the device. At each increment, the difference between the pressure behind the ionic device and atmospheric pressure was determined along with volumetric air flow. Also, at each point, voltage and current to the ionic air moving device were measured. These data were used to generate P-Q curves, as well as to generate efficiency curves.

P-Q and efficiency curves were generated at various incremental distances between the pins and the ring. This was done with a 10mm thick ring, a 6 mm thick ring, and a 4mm thick ring. At each distance, the voltage was increased incrementally, and air flow measured at each increment until either sparking occurred or the voltage limit of the power supply was reached. If sparking occurred, the voltage was reduced to the point of maximum air flow but below the voltage where sparking occurred. Finally, distance was fixed and air flow was set at 2.16 CFM. Ring width and number of ionization sites were varied while keeping the maximum air flow constant. Efficiency was then calculated at each point on the P-Q curve. Static efficiency (η) was calculated as,

$$\eta = P*Q/V*I \qquad (4.1)$$

where P = back pressure, Q = volumetric flow, V = voltage across the ring and needle, and I = current.

4.2 Results

As distance from the pins to the ring was increased, the voltage at which sparking occurred increased until the limit of the power supply (24800 V) was reached. Figure 4.3 shows the maximum observed air flow at each distance from the needles to the closest point on the ring. Each needle was equidistant from the ring. Even though voltage was increased at each increment in distance, the rate of change of air flow decreases, reaching a peak value.

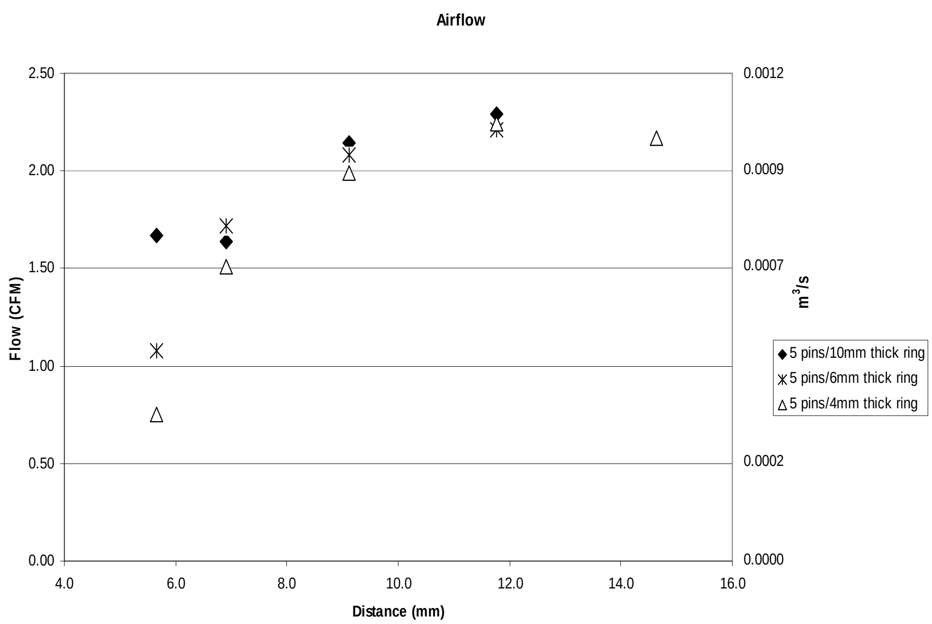

Figure 4.3 Air flow as a function of distance and ring thickness. Maximum air flow was obtained by increasing voltage at each point until just before the onset of arcing or until the limit of the power supply (24800 V) was reached. Air flow trends toward a peak at around 12mm.

Figure 4.4 shows results for air flow in the case where distance was increased while voltage was maintained at the upper limit of the power supply (24800V). Air flow decreased with distance in this regime, but efficiency increased as shown in Figure 4.5.

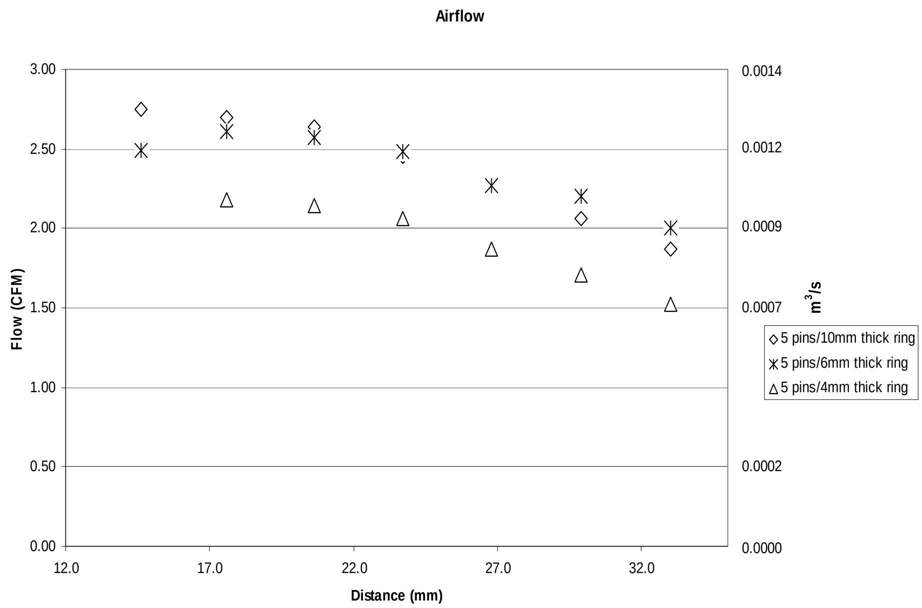

Figure 4.4 Air flow as a function of distance and ring thickness at fixed voltage . The limit of the power supply (24800 V) had been reached, so could not be increased as distance was increased. Air flow steadily decreases with distance.

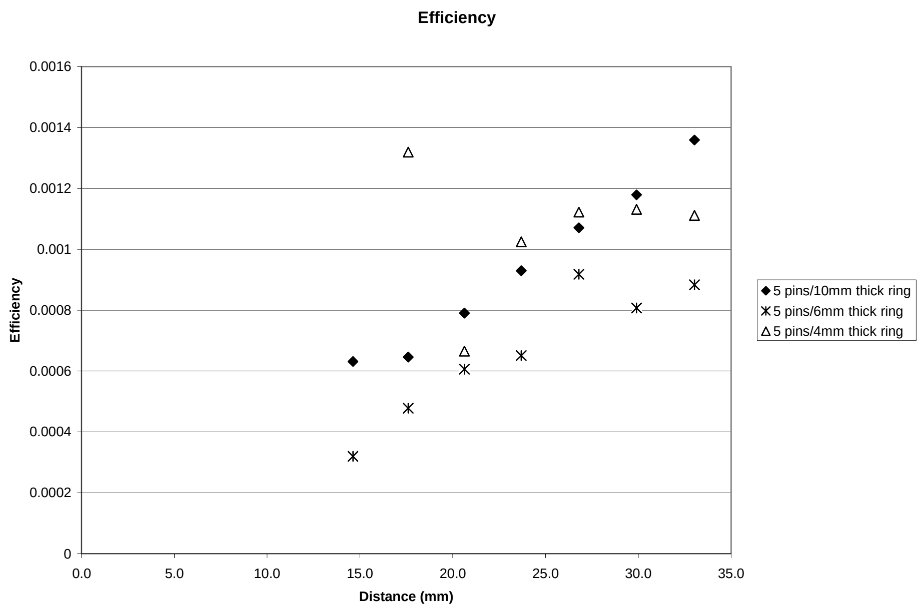

Figure 4.5 Efficiency as a function of distance and ring thickness at fixed voltage . The limit of the power supply (24800 V) had been reached, so could not be increased as distance was increased. Efficiency steadily increases with distance.

Figure 4.6 shows a set of efficiency curves over the operating range of the device at various voltages. It shows that at a given distance, as voltage increased air flow also increased, but efficiency decreased.

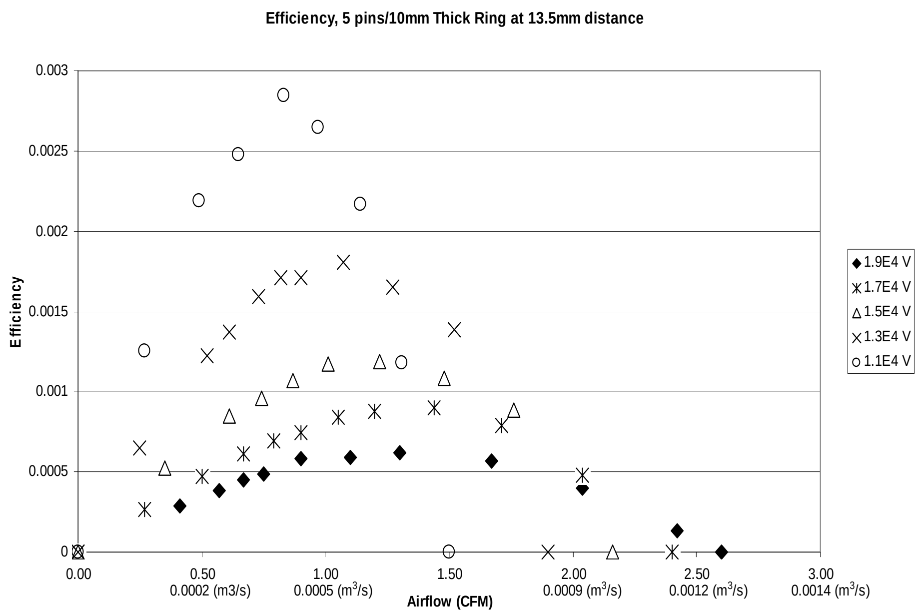

Figure 4.6 Efficiency curves at various voltages and fixed needle distance of 13.5mm. Efficiency decreased throughout the operating range of the air moving device as voltage was increased while maximum air flow increased.

In Figure 4.7, voltage is fixed for the set of curves, but the width of the ring was varied. In this case, there was no clear difference between the 10 mm and 6 mm ring, but the 4 mm ring showed lower flow and higher efficiency. Figure 4.8 is similar, but the number of ionization sites was varied rather than the ring width. Figure 4.8 shows that an increase in ionization sites allows higher voltage and air flow, but at lower efficiency.

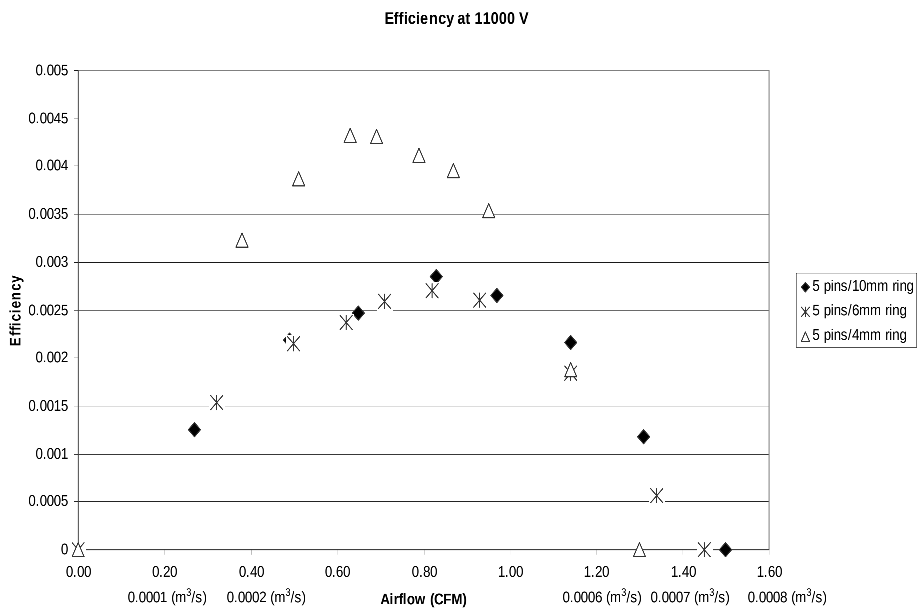

Figure 4.7 Efficiency at various ring widths at constant voltage. Air flow increased as ring size was increased, as long as the increase was larger than the uncertainty of the measurements.

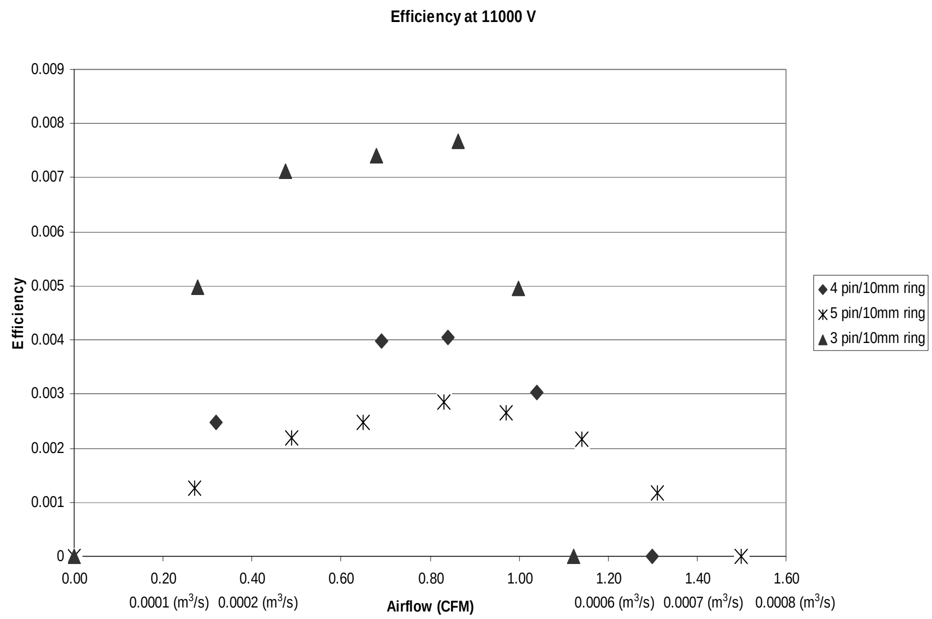

Figure 4.8 Efficiency with 4 and 5 ionization sites (needles). As in Figure 10, air flow increased as ionization sites were increased, but efficiency decreased.

Figure 4.9 shows that when maximum air flow was held constant, and the ring width was varied, efficiency was higher for the 10mm ring, but no clear trend was seen between the 4 mm and 6 mm rings. Figure 4.10 shows that when air flow was held constant similar to Figure 4.10, but the number of ionization sites was varied, efficiency increased with the number of ionization sites.

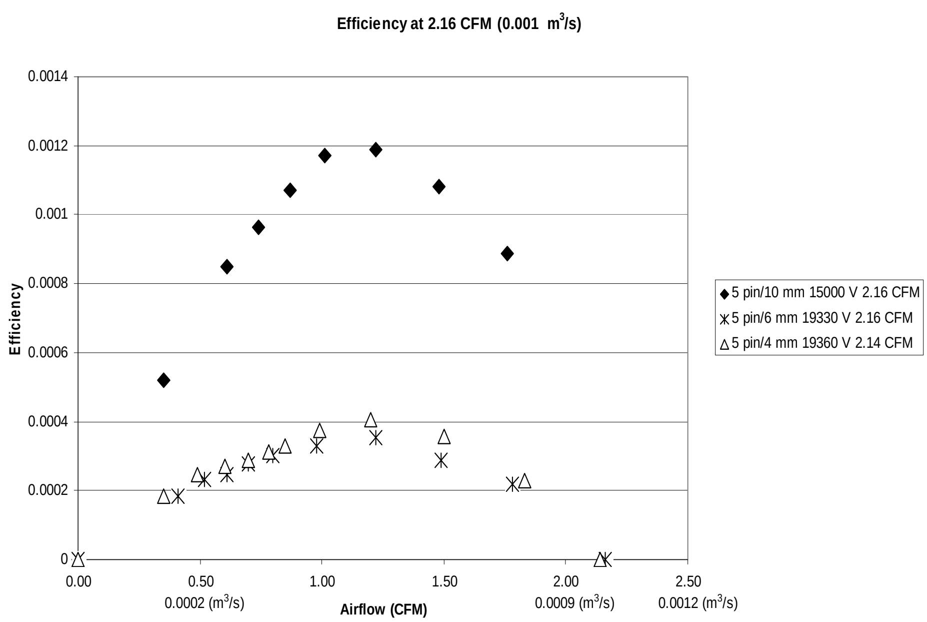

Figure 4.9 Efficiency of different ring widths at a fixed maximum air flow. Efficiency increased with ring thickness when air flow was held constant.

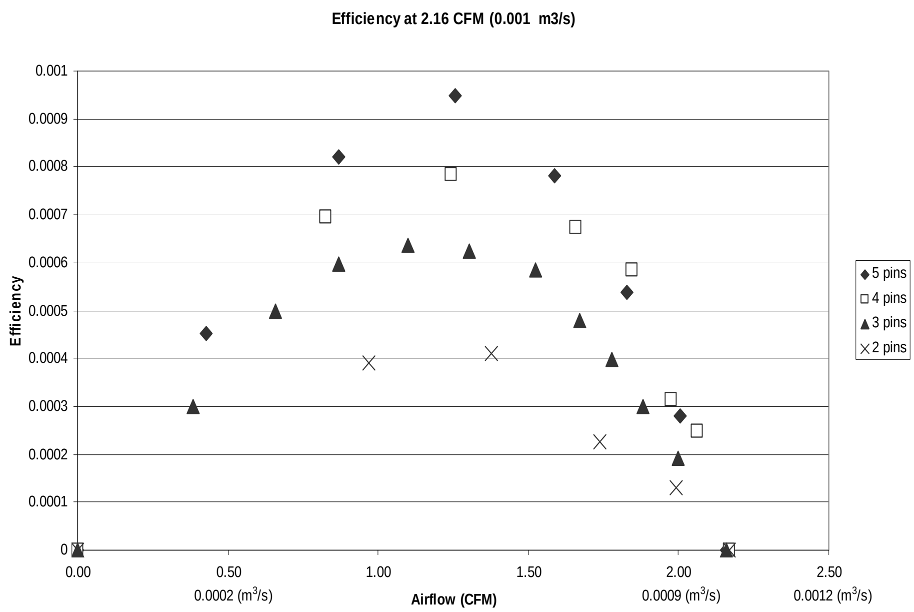

Figure 4.10 Efficiency of 4 and 5 ionization sites at a fixed maximum air flow. Efficiency increased with number of ionization sites when air flow was held constant.

4.3 Discussion

The P-Q curve is a common tool for determining the performance of an air moving device. At the origin, flow is zero and pressure is at its maximum. At this point, efficiency is necessarily zero. Also, at the point of maximum flow, pressure is zero, and therefore efficiency is zero as well. Efficiency peaked near the midpoint of the PQ curve for the air moving devices in this study. For Figures 4.3, 4.4, and 4.5, P-Q and efficiency curves were generated at each distance, then maximum efficiency or maximum flow was determined. Figures 4.6-4.10 show the entire efficiency curve.

As ring width was increased, efficiency increased as long as air flow was held constant. Increased ring width also allowed for voltage to be increased before sparking occurred at a given distance. This led to higher air flow, but lower efficiency. More ring widths need to be tested to determine the optimal width, and therefore optimal efficiency. While increasing the ring width could be used to increase air flow or efficiency, a point would be reached where friction would begin to dominate and air flow or efficiency would begin to decrease. It appears as though efficiency was very sensitive to voltage, as increases in voltage generally decreased efficiency. These trends are not clearly illustrated in Figure 4.3 due to the difficulty of determining maximum air flow from the point at which sparking occurs. Sparking is influenced by factors such as humidity, and surface imperfections on the ring. Once sparking had occurred, it happened more frequently and at lower voltage since it tended to cause marks on the surface of the ring where the spark hit. These marks then were observed to be the origin of subsequent sparks, even after the ring was rotated relative to the needles. In subsequent experiments, the rings were removed, cleaned, and polished to their original surface finish to reduce this effect.

When voltage and distance were increased such that the maximum air flow was obtained prior to the onset of sparking, flow peaked at a value around 12 mm. In the fixed voltage regime in this study, efficiency was seen to increase with distance past 20 mm, while air flow steadily decreased. This suggests that there is an inverse relationship between air flow and efficiency past a certain distance. This experiment should be repeated at constant voltage at lesser distances, as well as greater distances since efficiency cannot be expected to increase without bound.

In Figure 4.7, it was shown that efficiency was highest for the 4mm ring due to lower voltage, and therefore lower maximum air flow. It would them be expected that efficiency for the 6mm ring would lie between the values for the 4 mm and 10 mm ring. Instead, the values for those rings are very close together. This was likely due to the effects of sparking as mentioned previously, as well as accuracy issues with measurement of the very small air flows observed. Figure 4.9 shows similar behavior.

When the number of ionization sites was varied, more sites allowed for higher voltage and therefore higher flow. However if the maximum air flow was held constant, more ionization sites resulted in higher efficiency. The apparatus only allowed for up to 5 pins, however 5 pins does not appear to be a limiting number. The increase in efficiency between 2, 3, 4, and 5 pins suggests that the efficiency would still increase with 6 pins. Since efficiency cannot increase unbounded with the number of pins, it is assumed that there would be some number of pins where the efficiency no longer increased. Further work needs to be done with a modified apparatus and more pins.

4.4 Conclusions

The results of this study show how variation in collector width, and in the number of ionization sites influences the efficiency and air flow. Also, the data suggest that efficiency is sensitive to voltage.

1) When voltage was increased to a maximum with each increase in distance, air flow reached an optimal value.

2) When voltage was held constant as distance was increased, flow decreased and efficiency increased with distance.

3) When voltage was increased to a maximum with each increase in ring thickness, or with an increase in number of ionization sites, flow increased and efficiency decreased. However if air flow was held constant as ring thickness or number of ionization sites were increased, voltage needed to maintain the flow decreased and efficiency increased.

Chapter 5

Excerpts from:

M.S. June, J. Kribs, K.M. Lyons, Measuring Efficiency of Positive and Negative Ionic Wind Devices for Comparison to Fans and Blowers, Submitted for Review to Journal of Electrostatics 08/02/2010

5.1 Procedure

An ionic air moving device consisting of aluminum cylinders of various lengths, all 25.4 mm inside diameter and 5 x 1.3 mm diameter sewing needles as the emitters were used in this study. The needles were held in an aluminum fixture on a 12.2 mm diameter circle. Figure 5.1 shows a side view of the apparatus attached to a flow bench. Figure 5.2 shows the needle holder rotated away from the ring.

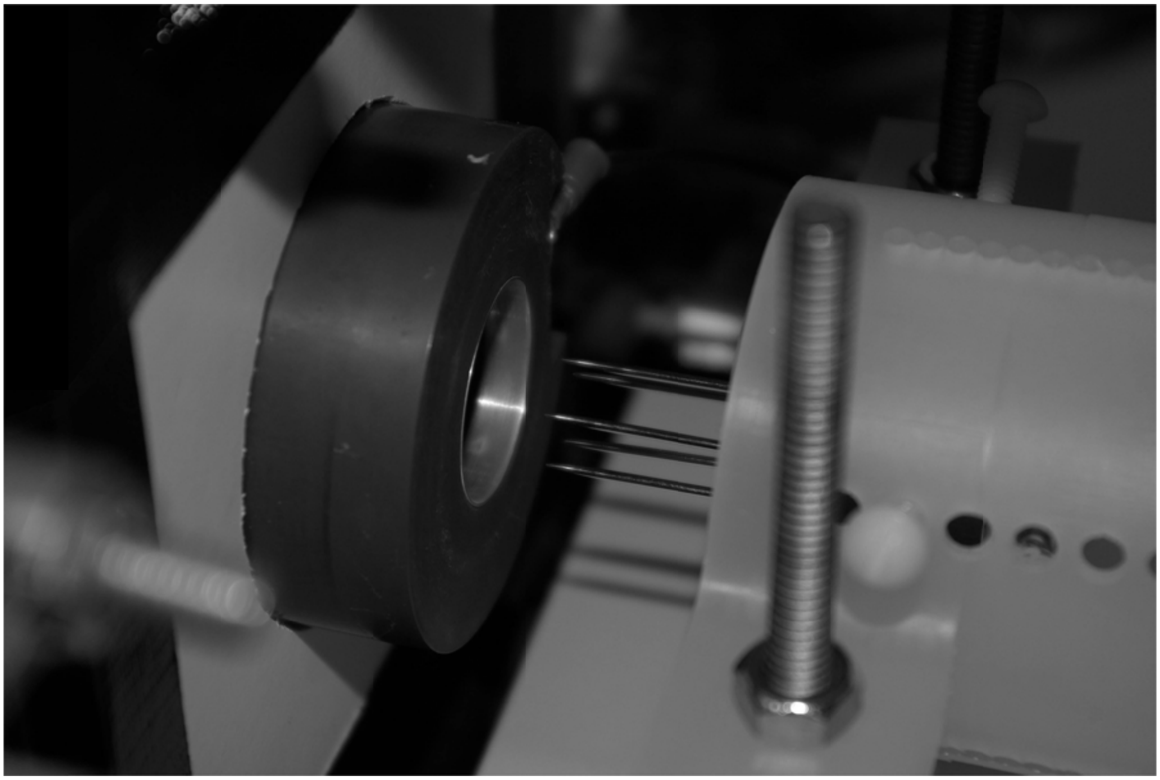

Figure 5.1 Photograph of experimental apparatus showing the ring electrode and 5 needle electrodes.

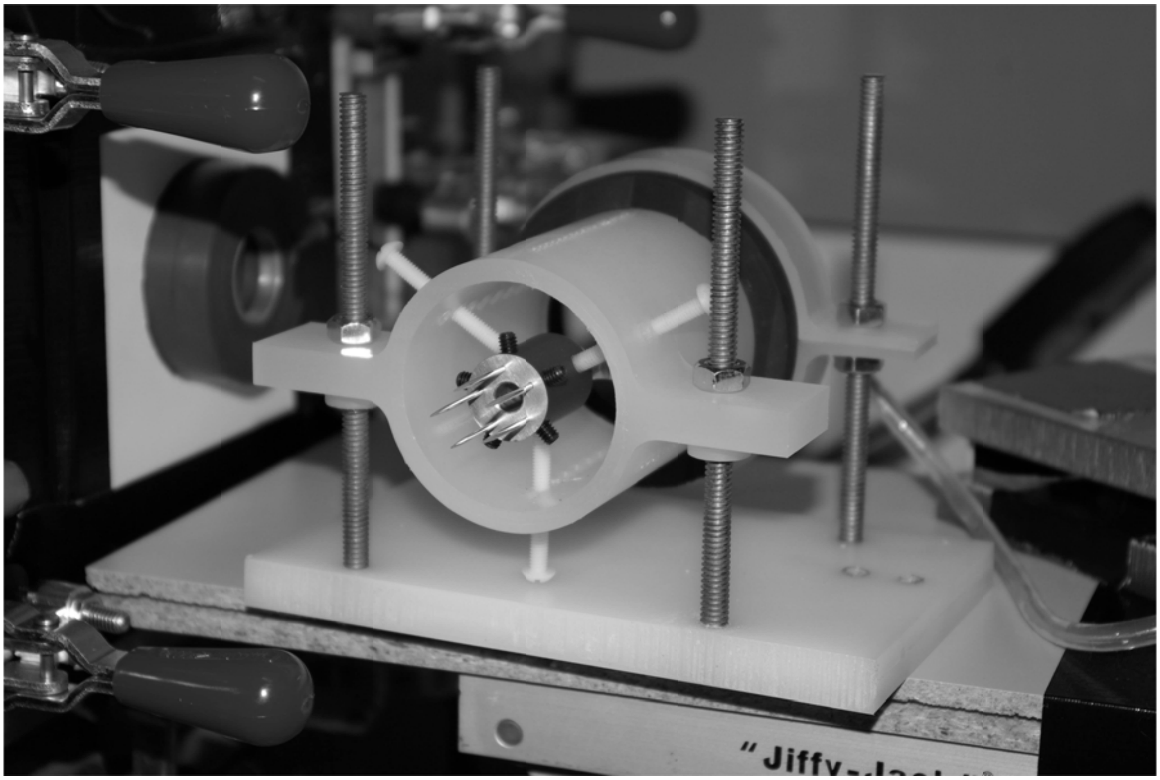

Figure 5.2 Photograph of experimental apparatus with the needle electrodes rotated 90-degrees to show the arrangement of the needles.

A 20kV Acopian DC power supply was used to supply a potential between the needle and the ring. A negative potential was applied to the needles, and the aluminum ring was grounded. For positive ionic flow, the negative potential was applied to the ring, and the needles were grounded.

Air flow and static pressure were measured using a typical air flow bench (Figure 5.3). An air flow bench consists of an air flow source, in this case a centrifugal blower, to evacuate air from a Lexan chamber. Between the blower and the chamber is a ball valve to regulate air flow, and typically a calibrated orifice of some type to measure volumetric air flow leaving the chamber. Additionally there is a pressure sensor to detect the static pressure in the chamber relative to atmospheric pressure The device under test is configured to blow into the chamber. Initially the air flow out of the chamber is adjusted until there is a reading of zero static pressure. At this point it is assumed that the air flow out of the chamber is equal to the flow into the chamber and thus the open flow rate of the device is determined. The valve is then closed in increments to simulate various loads on the AMD. At each point static pressure and air flow are determined. This is continued until the valve is fully closed. This is the point of maximum static pressure and zero air flow. At each point the voltage and current supplied to the AMD is recorded, and static efficiency is determined from these data.

For the current study, static pressure was measured with a Setra 339-1 digital manometer. Volumetric air flow was measured with a Miriam 50MW20-1F linear flow element (specific use of linear flow element in this manner is subject to pending US Patent owned by IBM) and a Datametrics 1018 differential manometer. Voltage to the ionic device was measured using a Hewlett Packard HP3468A DMM attached to the voltage sense terminals of the Acopian power supply. Current was measured also using a Hewlett Packard HP3468A DMM attached to the current sense terminals on the Acopian power supply. The voltage sense terminals output 1 V for every 10,000 V power supply output and the current sense terminals output 1 V for every 1mA power supply output.

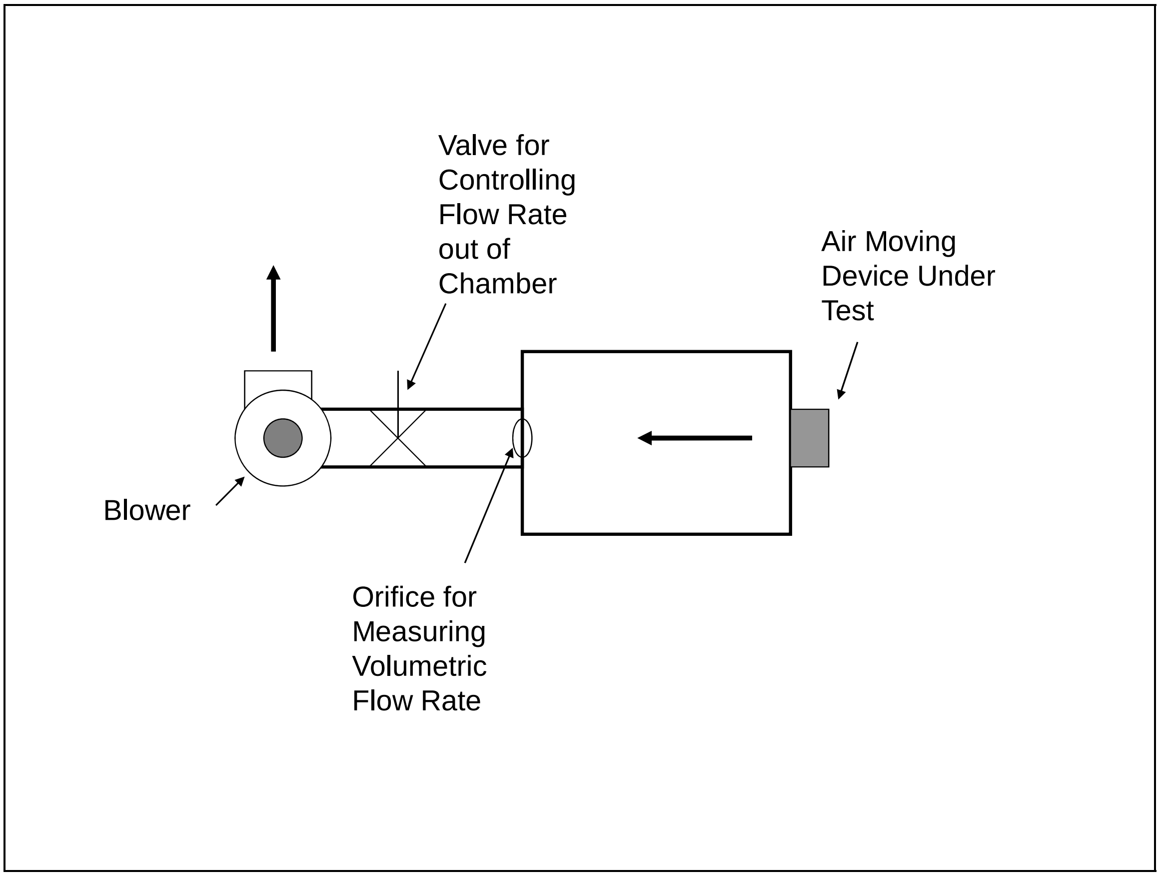

Figure 5.3 Schematic representation of typical air flow bench.

Performance and efficiency curves were generated at various incremental distances between the pins and the ring. This was done with 6, 8, 10, and 14 mm long cylinders for positive ionic flow, and with 6, 8, 10, 14, 20 and 26 mm long cylinders for negative ionic flow. Dunn-Rankin *et al* reported that the optimal flow was achieved at a needle to cylinder distance of r, where r is the needle to cylinder distance. Distances were chosen around this value. Cylinder lengths were also chosen around an optimal value given by Dunn-Rankin for air flow velocity of $\sqrt{2} \cdot r$. Initial work showed that the highest efficiency was achieved at lower voltages, so at each distance, the voltage was adjusted until the stagnation pressure of the device was 1.5 PA (0.006 in-H20). This was to ensure that the static pressure measurement stayed above a reasonable lower detection limit for that instrument.

5.2 Results

Figure 5.4 shows that as air flow and therefore voltage is increased, peak efficiency falls quickly, but appears to level off at higher flows. For efficiency comparison as function of needle distance, it would be desirable to run the device at the conditions corresponding to the flat part of the curve. This would reduce the effects of voltage variation on the efficiency numbers. Unfortunately, at short distances sparking occurred before the flat part of the curve was reached. Also this approach would give a minimum efficiency, rather than a maximum efficiency. Instead, efficiency data was taken at the minimum air flow and pressure detectable by the instrumentation which would result in a sufficient number of accurate data points to construct a flow curve and calculate peak efficiency. Figure 5.5 shows a characteristic performance curve as well as an efficiency curve for the ionic flow device used in this study. In this study, peak efficiency was defined as the highest point on the efficiency vs air flow curve, and maximum air flow was defined as the air flow at zero static pressure (open flow).

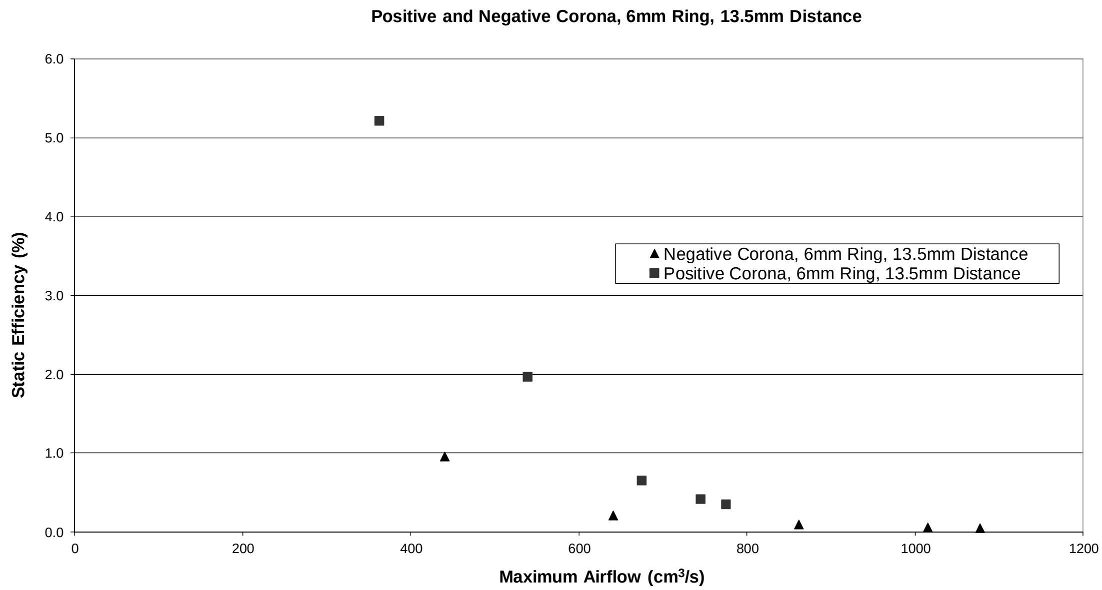

Figure 5.4 Behavior of peak static efficiency as a function of air flow, and therefore voltage. For lower air flows, positive corona yielded much higher efficiencies than negative corona. The static efficiency dropped quickly with air flow, and curves for both polarities showed the same nature. Higher peak air flows were achieved with negative coronas, as the positive coronas tended to arc at lower voltages.

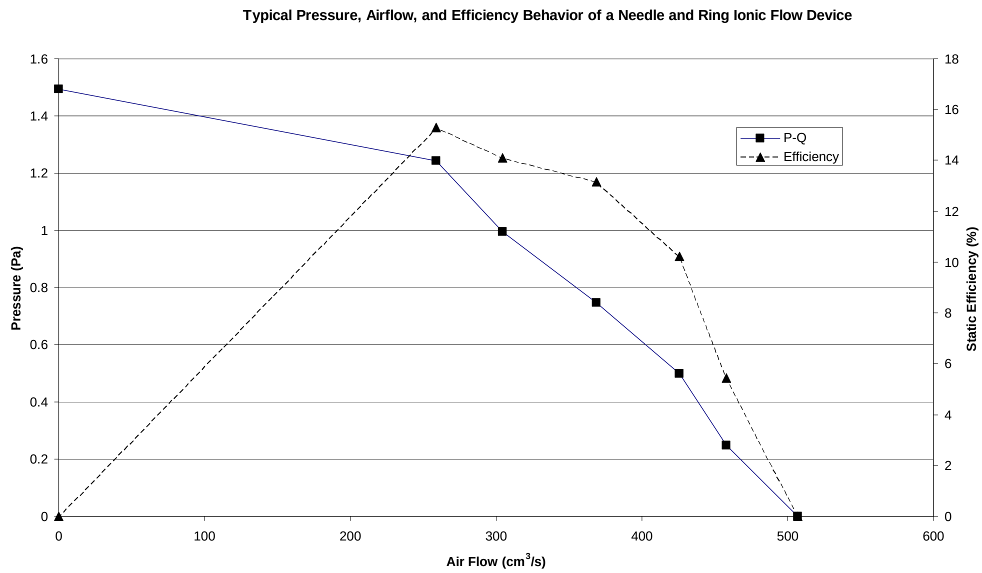

Figure 5.5 Characteristic performance curve for a needle-ring ionic flow device, as well as characteristic static efficiency curve. Lines were added for clarity.

Figure 5.6 shows peak static efficiency for needle to ring perpendicular distances from 3 mm to 47 mm with a negative ionic flow. Similar data were generated for various ring widths from 8 mm to 26 mm. Clearly, static efficiency peaks around 19 mm distance, and for the 14 mm thick ring. Figure 5.7 is similar to Figure 5.6 however with a positive ionic flow. There is still a peak around 19 mm distance, but the peaks are clipped at the detection limit of the current measurement technique. For this reason, ring thicknesses greater than 14 mm were not tested.

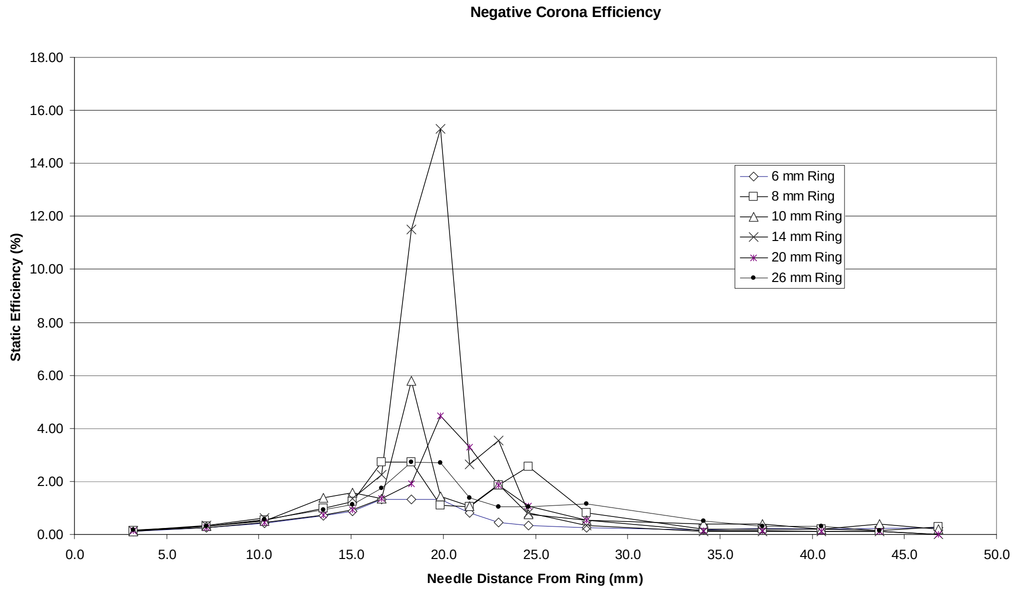

Figure 5.6 Negative corona static efficiency as a function of distance from the needle to the upstream plane of the ring, for 6 different ring lengths. Static efficiency showed sensitivity to distance, and peaked at approximately 20 mm. The most efficient ring length was 14 mm. Lines were added for clarity.

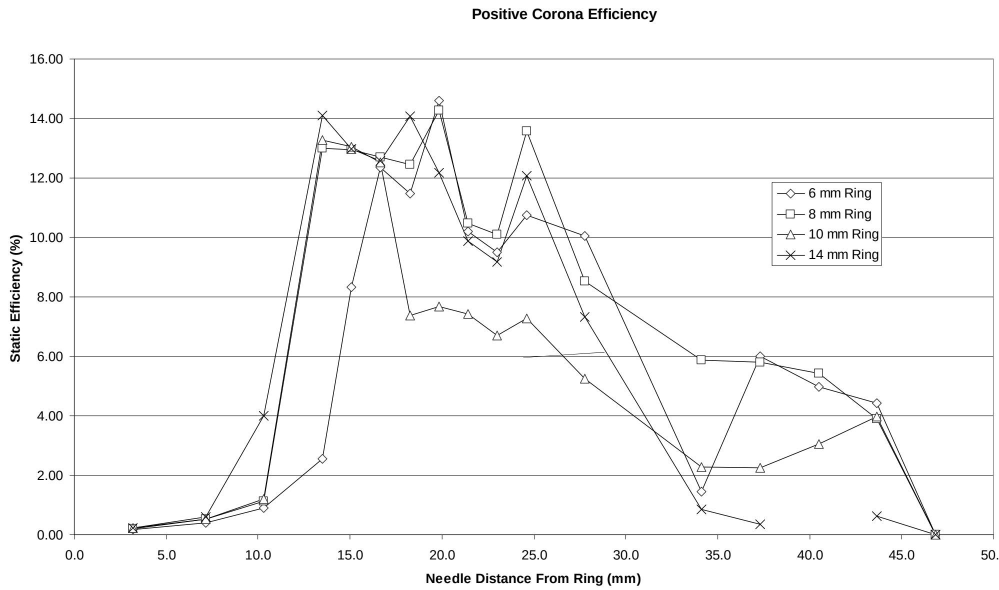

Figure 5.7 Positive corona static efficiency as a function of distance from the needle to the upstream plane of the ring, for 4 different ring lengths. Measurements of current were at or below the detection limit of the measurement methodology, and therefore values at the expected peak are all similar showing no trend. For this reason, only 4 rings lengths were tested. Lines were added for clarity.

Figure 5.8 shows a comparison of positive and negative ionic flow static efficiency for a 6 mm thick ring. Static efficiency was much higher for positive ionic flow than for negative ionic flow. This result was observed for all ring widths except for the 14 mm ring. This was likely due to the positive static efficiency curve being clipped. Figure 5.9 shows that efficiency as a function of collector length peaks around 14 mm.

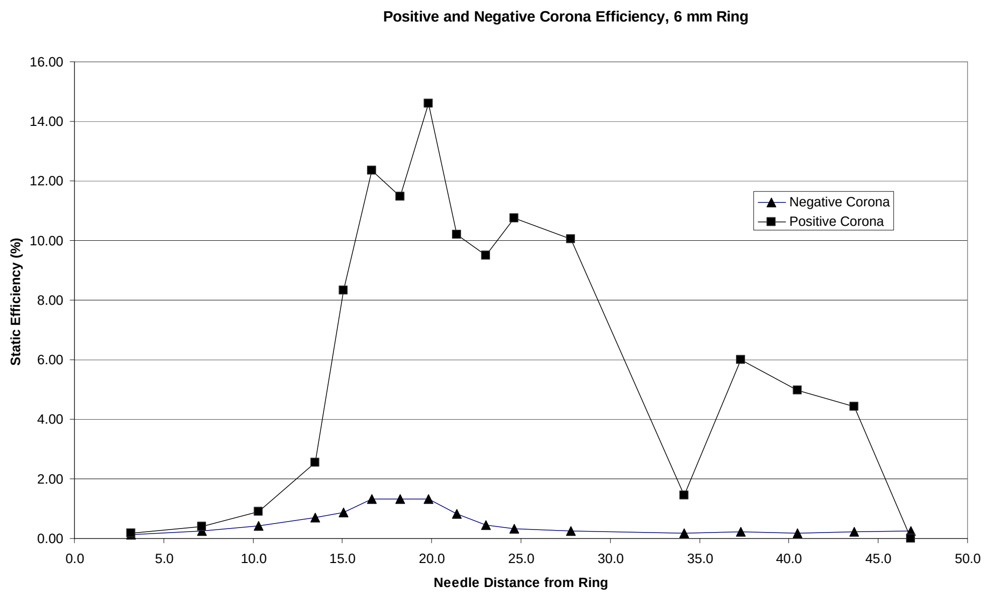

Figure 5.8 Comparison of positive and negative corona static efficiency for a ring length of 6 mm. This was a lower efficiency ring length in the negative corona data, and therefore was low enough to be above the detection limit of the current measurement methodology. The trend for positive corona static efficiency to be much higher than the negative case, as well as the peak for both around 20 mm distance can be seen. Lines were added for clarity.

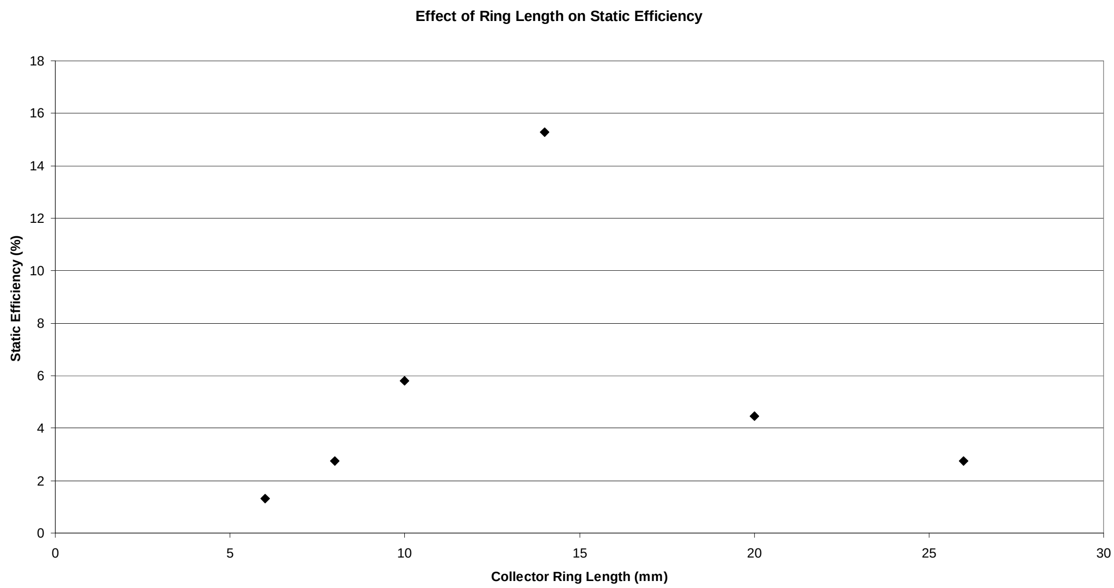

Figure 5.9 Static efficiency as a function of ring length. This shows the sensitivity of static efficiency to ring length, where the peak occurred with the 14 mm long ring.

5.3 Discussion

Figure 5.6 shows a peak in the data around 19 mm distance from needle to ring. This was 18 mm from the needles to the plane of the ring, not to the ring itself. The actual distance to the leading edge of the ring was 19 mm due to the needles being on a 12.2 mm diameter circle concentric to the 25.4 mm inside diameter ring. There was a dramatic increase in efficiency around this distance, implying that efficiency had a great sensitivity to distance. Dunn-Rankin et al (2007) found that the optimal needle to cylinder distance for air flow was r (r = 13 mm in this study). In a previous study by the authors of this paper (June et al, 2010) it was found that the maximum air flow occurred with the same apparatus used in this study at r =13 mm as expected, but the results of the current study show efficiency peaked at a distance of 19mm. This results in a needle to nearest point on the collector distance for maximum efficiency of $\sqrt{2.5} \cdot r$. Static efficiency was also sensitive to length of the collector, as efficiency peaked around a length of 14 mm. At lengths greater than 14 mm friction between the walls of the collector and the air began to dominate the other losses. Dunn-Rankin et al (2007) found that the optimal cylinder length was $\sqrt{2} \cdot r$. In the current study $\sqrt{2} \cdot r =$ 18 mm. It was found that optimal efficiency occurred for a cylinder length of 14 mm. Once again showing that the geometry that gives maximum flow may not give maximum efficiency. It should be noted that around this value of 18 mm, only a 14 mm and a 20 mm cylinder were tested. It is possible that the highest efficiency would have been observed between 14 mm and 20 mm. Cylinder lengths of 15 mm through 20 mm in 1 mm increments need to be tested to determine a good correlation for efficiency. Finally, the positive corona was much more efficient at producing flow, than the negative corona. This was as expected since the negative corona is pulsitile while the positive corona is steady (Trichel, 1938). The negative produces the maximum number of ions periodically for an apparently steady current and voltage , while the positive corona steadily produces its maximum number of ions. The positive corona was so efficient that the current fell below the detection limit of the instrumentation. This resulted in the aforementioned clipped peaks in the efficiency graphs (Figure 5.7). Measuring current in the pico-amp range is know to be problematic, and will be addressed in subsequent studies.

5.4 Conclusions

The results of this study show the sensitivity of static efficiency of ionic air moving devices to emitter distance, length of the collector, and to polarity of the electrodes.

1) Static efficiency peaked when the distance from the emitter to the collector was $\sqrt{2.5} \cdot r$. This does not coincide with the distance that provides maximum air flow (reported by Rickard, Dunn-Rankin, Weinberg (2006) as r).

2) Static efficiency peaked when collector length was 14 mm. This does not coincide with the length that provides maximum air flow (reported by Rickard, Dunn-Rankin, Weinberg (2006) as $\sqrt{2} * r$).

3) Static efficiency of the positive ionic flow was significantly higher than the negative ionic flow for a given emitter distance and collector length.

Chapter 6

Excerpts from:

M.S. June, J. Kribs, K.M. Lyons, Integrated Ionic Flow Device and Heat Sink as a Fan Sink Alternative, Submitted for Review to Journal of Thermal Science and Engineering 6/18/2010

6.1 Procedure

A small aluminum extruded profile heat sink was placed on a circular cartridge heater, and placed in a flow bench. The overall dimensions of the heat sink were 31 mm length x 31 mm wide x 28 mm tall with a base thickness of 2 mm (26 mm tall fins). There were 12 fins, each 0.9 mm thick with 2mm spacing. There was a 4 mm space between the center two fins. Air flow to the heat sink was provided by either a 25 mm axial fan, or by integrating an ionic air flow device. The ionic device consisted of 5 common 1.3 mm sewing needles

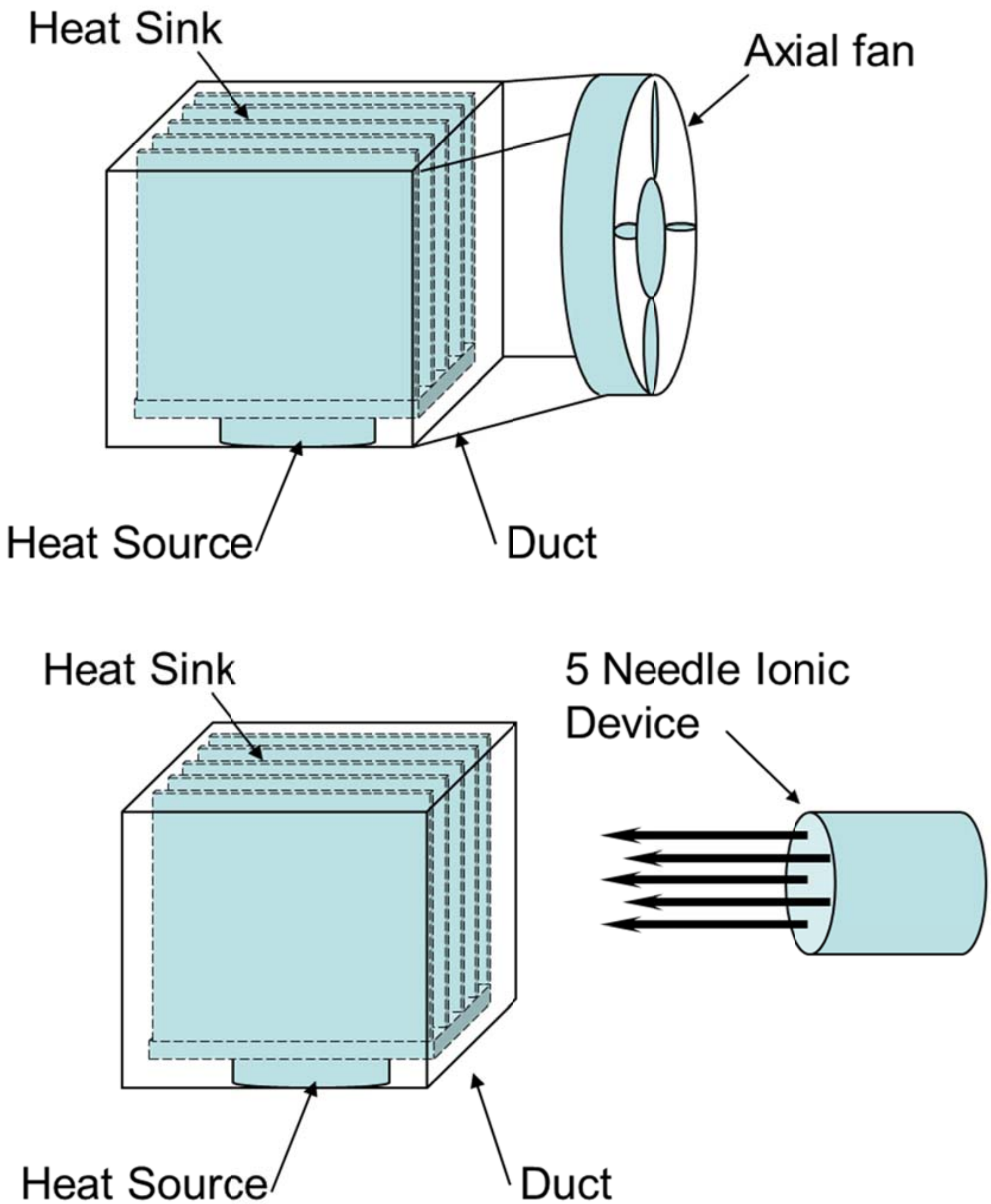

Figure 6.1 Sketch of the heat sink ducted to the axial fan, and the heat sink as part of a 5 needle ionic air moving device.

A 20kV Acopian DC power supply was used to supply a potential between the needle and the heat sink for the ionic device. For negative ionic flow, negative potential was applied to the needles, and the aluminum heat sink was grounded. For positive ionic flow, the negative potential was applied to the heat sink, and the needles were grounded.

Air flow was measured using a flow bench consisting of an air flow source and a chamber. Air flow through the chamber was balanced with air flow from the ionic air moving device by closing a valve between the air flow source and the chamber. When static pressure in the chamber was zero, the air flow into the chamber from the ionic device was the same as the air flow out of the chamber from the air flow source. Static pressure was measured with a Setra 339-1 digital manometer. Volumetric air flow was measured with a Miriam 50MW20-1F linear flow element and a Datametrics 1018 differential manometer.

At each point, voltage and current to the ionic air moving device were measured. These data were used to generate the P-Q curves used to determine static efficiency. Voltage to the ionic device was measured using a Hewlett Packard HP3468A DMM attached to the voltage sense terminals of the Acopian power supply. Current was measured also using a Hewlett Packard HP3468A DMM attached to the current sense terminals on the Acopian power supply. The offset for voltage readings was 1 V indicated for 10,000 V output. For the current measurement, 1 V indicated 1 mA output.

Since efficiency is a function of distance between the emitter and the collector, this distance was varied from 11 mm to 35 mm and static efficiency was determined at seven increments to determine the optimal distance.

Heat was applied to the heat sink using a 19 mm diameter circular heater with thermal grease between the heater and the heat sink. The heat sink base temperature was measured with a thermocouple when evaluating the fan.

The fan was fully ducted to the heat sink when placed on the flow bench. The fan was powered up along with the heater, and the temperature of the heat sink base in the middle of the heater was measured with the thermocouple. The air flow through the heat sink was measured using the flow bench, and the power used by the fan was noted. The fan was then removed, and the 5 needle ionic device was assembled, and powered to the same air flow as the fan. Power used by the ionic air flow device was measured by noting the voltage and current drawn by the device.

6.2 Results

With the axial fan at full speed, fully ducted to the heat sink, the thermal resistance from the base to the air was 1.9 C/W. This was achieved with the fan consuming 0.4W of electrical power. The air flow through the heat sink was 462 cm^3/s (0.98 SCFM). The heater supplied 17W of power.

Figure 4 shows the static efficiency of the ionic device using the heat sink as the collector, for various needle to heat sink distances. Based on these data, the needles were placed 21 mm in front of the heat sink for both the positive and negative ionic device.

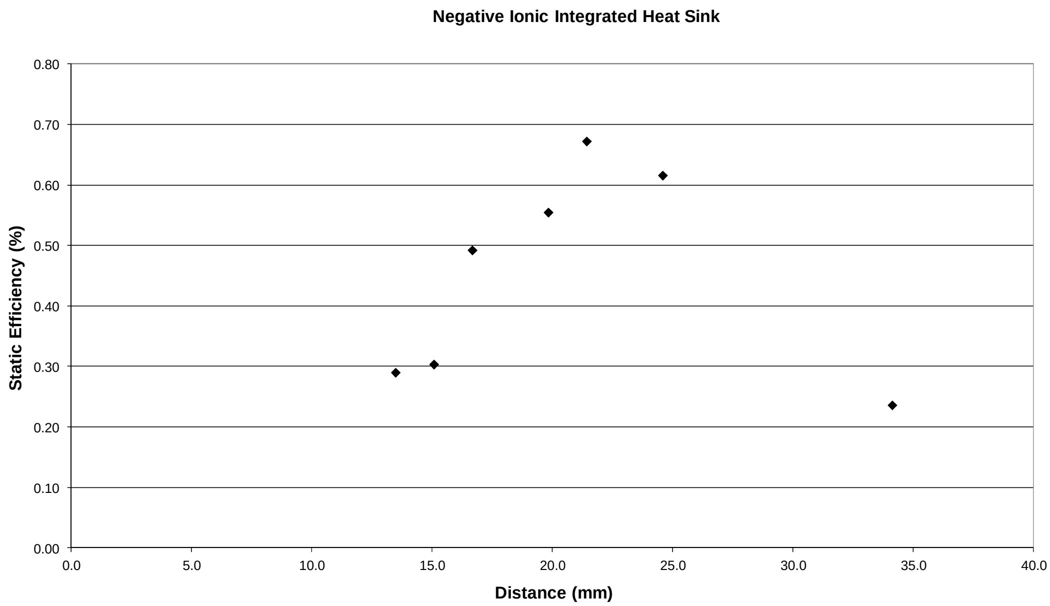

Figure 6.2 Static efficiency as a function of distance between the needle and the heat sink. Static efficiency peaks at a distance of 21 mm between the needles and the heat sink.

The 5 needle positive ionic device consumed only 0.19 W at 462 cm^3/s through the heat sink. Subsequently the device was reconfigured as a negative ionic device and was tested at 462 cm^3/s, consuming 0.17W.

Table 6.1 Comparison of power consumed by each air moving device at 462 cm^3/s air flow.

Device	Airflow	Power
	(cm^3/s)	(W)
25 mm Axial Fan/ Heat Sink	462	0.40
Negative Ionic Device/ Heat Sink	462	0.19
Positive Ionic Device/ Heat Sink	462	0.17

6.3 Discussion

The ionic devices both consumed less power than the fan when cooling a simulated low power electronic component at 17W heat output. In computer systems, devices of concern in this power range generally have to be kept below 85C at the silicon level. The temperature at the heat sink base is typically 70C when the silicon is at 85C, assuming typical thermal resistances from the silicon to the point of measurement on the heat sink base. Heat sink base temperature was measured only for the axial fan cooled heat sink due to difficulties with thermocouple measurement and ionic devices. The negative ionic device induces enough voltage in the thermocouple wire to cause significant inaccuracy. Since the needles were grounded on the positive ionic device, the thermocouple would have been at the same high potential as the heat sink, rendering it unreadable in that case as well. For these reasons, air flow was held constant between the three cases, and the assumption was made that the heat sink base temperature would be the same given the same air flow, ambient conditions, and heater power.

6.4 Conclusions

The results of this study show the ionic air moving device used less power than a comparable axial fan to cool a low power electronic component.

1) At 462 cm^3/s (0.98 SCFM), the negative ionic AMD required 0.17W while the axial fan required 0.40W

2) The negative ionic device consumed slightly less power than the negative device (0.17 W vs 0.19 W) at equivalent air flow, but both consumed less than half the power as the fan.

3) The stated flow conditions and heat sink were sufficient to cool at 17W component to a reasonable temperature of 70C at an ambient condition of 35C and 3000ft altitude. This is a typical upper bound for computer equipment.

Chapter 7

Discussion and Future Work

7.1 Overall Summary of Results

The results of the previous three studies show how variation in collector length, and the number of ionization sites influences the efficiency and air flow. Also, the data suggest that the efficiency is very sensitive to voltage. Static efficiency of ionic air moving devices depends strongly on emitter distance, and polarity of the electrodes as well. The results of the third study show the ionic air moving device used less power than a comparable axial fan to cool a low power electronic component.

Perhaps the most important conclusion that can be drawn from these studies is that when measured according to the same criteria as axial fans, the efficiency of ionic air moving devices compares much more favorably to axial fans than previously reported. While the data show that the pressure developed by these ionic devices is still low compared to axial fans and blowers, there is still much room for development and improvement. The following is a summary of the major results reported from the experiments.

1) When voltage was increased to a maximum with each increase in distance, air flow reached an optimal value.

2) When voltage was held constant as distance was increased, flow decreased and efficiency increased with distance.

3) When voltage was increased to a maximum with each increase in ring thickness, or with an increase in number of ionization sites, flow increased and efficiency decreased. However if air flow was held constant as ring thickness or number of ionization sites were increased, voltage needed to maintain the flow decreased and efficiency increased.

4) Static efficiency peaked when the distance from the emitter to the collector was between $\sqrt{2.5} \cdot r$. This does not coincide with the distance that provides maximum air flow.

5) Static efficiency peaked when collector length was 14 mm. This does not coincide with the length that provides maximum air flow.

6) Static efficiency of the positive ionic flow was significantly higher than the negative ionic flow for a given emitter distance and collector length.

7) At 462 cm^3/s (0.98 SCFM), the negative ionic AMD required 0.17W while the axial fan required 0.40W

8) The negative ionic device consumed slightly less power than the negative device (0.17 W vs 0.19 W) at equivalent air flow, but both consumed less than half the power as the fan.

9) The stated flow conditions and heat sink were sufficient to cool at 17W component to a reasonable temperature of 70C at an ambient condition of 35C and 3000ft altitude. This is a typical upper bound for computer equipment.

In general, the results show that these air moving devices can be more efficient than traditional air moving devices, and when incorporated into a heat sink, the system can be more efficient at removing heat than a traditional fan sink.

7.2 Future Work

While this work shows that ionic air moving devices are more promising alternatives to conventional rotary air moving devices than previously thought, there are still issues that need to be addressed. The following are suggestions for further research.

1) It was shown that air flow and efficiency increased with the number of ionization sites. It is trivial logic that the efficiency and air flow cannot increase without bound and therefore there must be an optimal number of ionization sites. Further investigation should include a needle holder that can hold many more than five needles.

2) The optimal number of ionization sites is hypothesized to depend on the collector area. This is from observations made in as yet unreported experiments with ionization sites and heat sinks of various fin areas. Therefore, the number of collector sites should be varied along with collector length to determine a relation.

3) Most air flow benches in use by fan manufacturers and by cooling system designers are set up for measuring static efficiency only. Measuring total efficiency would require addition of a dynamic pressure probe in accordance with ASME PTC 11-2008. This dynamic pressure measurement would enable further comparison of the literature's method of evaluating efficiency with the industry method. Since the derivations of both methods are based on first principles, and both derivations are validated and widely accepted, albeit by two different groups, the results should agree at some point. That point should be total efficiency at open flow. Static efficiency at open flow is zero, and the dynamic efficiency component is subtracted out, or ignored in the calculation and measurement of static efficiency. It is therefore the measurement of efficiency at open flow similar to the literature method. They should, therefore agree within reasonable uncertainty.

4) While ionic devices could be used as air moving devices in the general sense like fans and blowers, to provide system level air flow to many components, they have a major advantage over fans in that the cooled component can be made part of the air moving device. Typically, the impedance of the heat sink would be measured, also using a flow bench, to generate an impedance vs air flow chart. The fan performance curve is then overlaid onto this impedance curve to determine what flow rate a given fan can deliver to that particular heat sink. Comparison of fan

performance curves to comparable ionic devices shows that ionic devices are capable of much less air flow at a given pressure implying that ionic devices can't be an alternative to larger fans. However this is not a valid comparison, as when the heat sink is made the collector, it is no longer just impedance to the air flow. Rather it is a part of the air moving device actually generating the air flow. For this reason, traditional consideration of impedance and air moving device performance curves is invalid and must be replaced by a more appropriate metric. In unreported, preliminary experimentation it was observed that an array of needles set in front of a heat sink not optimized for ionic flow, generated enough flow to cool an 85 Watt CPU to reasonable operating temperatures, under reasonable ambient conditions. Looking at just the performance curves for that same needle array with a ring collector and the impedance curve for that heat sink, would never have led to the conclusion that it could cool an 85 Watt CPU. This work needs to be further carried out with an optimal heat sink geometry in terms of fin spacing, fin thickness, reduction of secondary ionization sites, and needle distance.

5) If there is some optimal number of ionization sites considering needles to be discrete ionization sites, it is hypothesized that for positive coronas, a long thin wire could hold a very long ionization site. Considering the number of ions generated to be proportional to the area of the corona discharge, there will be an

6) equivalent length of wire that will represent the same area as many needles. There is no data currently comparing the efficiency of a length of wire as an emitter, to an equivalent number of needles as emitters.

7) Currently the literature focuses on very small ionic air moving devices in the 25mm diameter range. This is a very inefficient size for axial fans. Larger axial fans can be anywhere from 10% – 45% efficient when over 40 mm in diameter. At 25 mm diameter they are around 0.5 % efficient. The previous studies need to be extended to larger ionic air moving devices. However, scaling the ionic devices to larger sizes will likely require geometry changes.

8) Ionic devices are known to emit ozone, which is potentially harmful to humans. Positive coronas produce noticeably less ozone than negative coronas, but for a device intended for consumer applications, these ozone emissions need to be carefully characterized and evaluated.

9) Ionic devices are known to emit electromagnetic interference which is potentially harmful to the electronics they are intending to cool. Positive coronas produce noticeably less interference than negative coronas, but this interference needs to be carefully characterized and evaluated.

10) Since these devices are also commonly used for air filtration, it is easy to imagine that fouling would be an issue for heat sinks used as part of the ionic air moving device. Control and minimization of fouling must be investigated in order to characterize the expected life or maintenance requirements of one of these systems before they will be widely adopted for electronics cooling applications.

7.3 Future Applications

This fan-less air moving technology is potentially valuable to electronic cooling applications due to its lack of moving parts, and comparably silent operation. It has been largely ignored by the computer industry due to its reported low efficiency and overall lack of development compared to conventional fans.

Renewed interest has been shown by the relatively new consumer LED lighting industry. The devices can be easily integrated into the design of the light fixtures, and with no moving parts and very quiet operation, they are a promising alternative to conventional devices. The challenge in these applications is control and minimization of fouling over long periods of time.

In addition to use of ionic air moving devices as primary air moving devices, they are also being investigated to enhance or to control air flow. As previously mentioned, research teams have been investigating boundary layer enhancement (Moreau, 2006; Go *et al*, 2008). Enhancements to efficiency of stand-alone ionic air moving devices also have applicability to these efforts as well.

There are many new potential applications for this somewhat ignored old technology. With further investigation into its fundamental principles and further development into practical devices, this technology shows more promise now than in the past. Moving this technology forward, however requires understanding of the issues with the technology that must be overcome by development engineers. It will also require that the metrics used to evaluate the technology are consistent with those used by the developers.

REFERENCES

Air Movement and Control Association International, Inc. and American Society of Heating, Refrigerating and Air-Conditioning Engineers, Inc., Laboratory Methods of testing Fans for Aerodynamic Performance rating, Arlington Heights, Ill. ANSI/ASHRAE Standard 51-1999, ANSI/AMCA Standard 210-99

American Society of Heating, Refrigerating and Air-Conditioning Engineers, Inc., Laboratory Methods of testing Fans for rating, Arlington Heights, Ill. ASHRAE Standard 51-75, AMCA Standard 210-74

American Society of Mechanical Engineers, Power Test Codes for fans, New York: ASME, Power Test Codes, PTC 11-2008

Bondar, H., Bastien, F. Effect of Neutral Fluid Velocity on Direct Conversion from Electrical to Fluid Kinetic Energy in an Electro Fluid Dynamics (EFD) Device, J. Phys. D. Appl. Phys., 19 (1986) 1657

Brown, N.M., Lai, F.C., Electrohydrodynamic Gas Pump in a Vertical Tube, J. Electrostat. 67 (2009) 709-714

Carleton, F.B., Weinberg, F.J., Electric field-induced flame convection in the absence of gravity, Nature 330 (1987) 635

Chakrabarty, R.K. et al, Morphology Based Particle Segregation by Electrostatic Charge, Aerosol Science 39 (2008) 785-792

Chattock, A.P., On the Velocity and Mass of Ions in the Electric Wind in Air, Phil. Mag. S. 5 48 (294) (1899) 401.

Chen, J., Davidson, J.H., Model of the Negative DC Corona Plasma: Comparison to the Positive DC Corona Plasma, Plasma Chem. Plasma Process. 23 (2003) 83

Dunn-Rankin, D., Weinberg, F.J., Using Large Electric Fields to Control Transport in Microgravity, Proceedings of the Interdisciplinary Transport Phenomena in Microgravity and Space Sciences Conference IV, Tomar, Portugal, August 7-12, 2005

Faraday, M., Experimental Researches in Electricity, London, England, pp. 665-1595, 1839.

Fox, R.W., McDonald, A.T., Introduction to Fluid Mechanics, Fourth ed.,Wiley, New York, 1992, pp. 544-618

Go, D., Garimella, S. V., Fisher, T. S., and Mongia, R. K., “Ionic Winds for Locally Enhanced Cooling,” Journal of Applied Physics Vol. 102, 053302, 2007

Goldman, M., Goldman, A., R.S. Sigmond, The Corona Discharge, Its Properties and Specific Uses, Pure Appl. Chem., 57 (1985) 1353

Hauksbee, F., Physico-Mechanical Experiments on Various Subjects, London, England, pp.46-47, 1709.

Jewell-Larsen, N.E., Hsu, C.P., Krichtafovitch, I.A., Montgomery, S.W., Dibene II, J.T., Mamishev, A.V., CFD Analysis of Electrostatic Fluid Accelerators for Forced Convection Cooling, IEEE Trans. on Dielectr. Electr. Insul., 15 6 (2008) 1745 – 1753

Jewell-Larsen, N.E., Parker, D.A., Krichtafovitch, I.A., Mamishev, A.V., Numerical Simulation and Optimization of Electrostatic air Pumps, 2004 Annual Report Conference on Electrical Insulation and Dielectric Phenomena , (2004) 106 -109

Jewell-Larsen, N.E., Ran, H., Zhang, Y., Schweibert, M.K., Honer, K.A., Mamishev, A.V., Electrohydrodynamic (EHD) Cooled Laptop, 25th IEEE SEMI-THERM Symposium, (2009) 261 – 266

Jewell-Larsen, N.E., Tran, E., Krichtafovitch, I.A, Mamishev, A.V., Design and Optimization of Electrostatic Fluid Accelerators, IEEE Trans. on Dielectr. Electr. Insul., 13 1 (2006) 191 – 203

June, M.S., Kribs, J., Lyons, K.M., Efficiency of Electrostatic Air Moving Devices, J. Electrostat, 68 (2010) 419-423

Kim, C., Park, D., Noh, K.C., Hwang, J., Velocity and Energy Conversion Efficiency Characteristics of Ionic Wind Generator in a Multistage Configuration, J. Electrostat. 68 (2010) 36-41

Komeili, B., Chang, J.S., Harvel, G., Ching, C.Y., Brocilo, D., Flow Characteristics of Wire-Rod Type Electrohydrodynamic Gas Pump Under Negative Corona Operations, J. Electrostat. (2008) 342 – 353

Komeili, B., Chang, J.S., Harvel, G., Polarity Effect and Flow Characteristics of Wire-Rod Type Electrohydrodynamic Gas Pump, 2006 Annual Report on Electrical Insulation and dielectric Phenomena, (2006) 182 – 185

Kroll, J., Gerhart, P.M., Jorgensen, R., A Comparison of Two Alternate Methods for Defining Fan Performance, J. Eng. Power, 104 (1982) 177-183

Lawton, J., Weinberg, F., Electrical Aspects of Combustion, Clarendon Press, Oxford, 1969

Maxwell, J.C., Treatise on Electricity and Magnetism, London, England, pp. 52-54, 1873.

Moreau, E., Airflow Control by Non-Thermal Plasma Actuators, J. Phys. D: Appl. Phys. 40 (2007) 605-636

Moreau, E., Touchard, G., Enhancing the Mechanical Efficiency of Electric Wind in Corona Discharges, J. Electrostat. 66 (2008) 39-44

Moreau, E., Leger, L., Touchard, G., Effect of a DC Surface-Corona Discharge on a Flat Plate Boundary Layer for Air Flow Velocity up to 25 m/s, J. Electrostat. 64 (2006) 215-225

Newton, I., Opticks, London, England, pp. 315-316, 1718.

Peek, F.W., Dielectric Phenomena in High Voltage Engineering, McGraw-Hill, New York, (1929)

Rickard, M., Dunn-Rankin, D., Weinberg, F., Carleton, F., Characterization of ionic wind velocity, J. Electrostat. 63 (2005) 711

Rickard, M., Dunn-Rankin, D., Weinberg, F., Carleton, F., Maximizing ion-driven gas flows, J. Electrostat. 64 (2006) 368

Rickard, M., Dunn-Rankin, D., Numerical simulation of a tubular ion-driven wind generator, J. Electrostat. 65 (2007) 646

Robinson, M., A History of the Electric Wind, Am. J. Phys. 30 (1962) 366.

Robinson, M., Movement of Air in the Electric Wind of the Corona Discharge, Trans. Am. Inst. Elec. Eng. 80 (1961) 143

Saito, M., Arai, T., Arai, M., Control of Soot Emitted from Acetylene Diffusion Flames by Applying an Electric Field, Combustion and Flame, 119 (1999) 356

Saito, M., Sato, M., Sawada, K., Variation of Flame Shape and Soot Emission by Applying Electric Field, Journal of Electrostatics 39 (1997) 305-311

Saxena, S.C., Henry, R.F., Podolski, W.F., Technology status of particulate removal from high-temperature high-pressure combustion gases, Aerosol Sci. and Technol., Vol. 1 Issue 2 (1982) 235

Steutzer, O.M., Ion Drag Pressure Generation, J. Appl. Phys., 30 (1959) 984-994.

Strayer, B.A., Posner, J.D., Dunn-Rankin, D., Weinberg, F.J., Simulating Microgravity in Small Diffusion Flames by Using Electric Fields to Counterbalance natural Convection, Proc. R. Soc. London Ser. A 458 (2002) 1151

Sylvestre de Ferron, A., Reess, T., Pecastaing, L., Gilbert, A., Domens, P., Pignolet, P.,Removal of Diesel Soot Particules [sic] using an ESP Supplied by a Hybrid Voltage, Eur. Phys. J. Appl. Phys. 43 (2008) 103-109

Takeuchi, N., Yasuoka, K., Efficiency of a Wire-Rod Type Electrohydrodynamic Gas Pump Under Negative Corona Operation, IEEE Transactions on Plasma Science, 37 6 (2009) 1021-1026

Thong, K.C., Weinberg, F.J., Electrical Control of Solid and Liquid Particulate Suspensions, Proc. Roy. Soc. Lond. A. 324 (1971) 201

Trichel, G.W., The Mechanism of the Negative Point to Plane Corona Near Onset, Phys. Rev., 54 (1938) 1078-1086

Tsubone, H., Ueno, J., Komeili, B., Minami, S., Harvel, G.D., Urashima, K., Ching, C.Y., Chang, J.S., Flow Characteristics of DC Wire-Non-Parallel Plate Electrohydrodynamic Gas Pumps, J. Electrostat. 66 (2008) 115-121

Weinberg, F., Carleton, F., Dunn-Rankin, D., Electric Field-Controlled Mesoscale Burners, Combust. Flame 152 (2008) 186-193

Weinberg, F., Carleton, F., Kara, D., Xavier, A., Dunn-Rankin, D., Rickard, M., Inducing gas flows and swirl in tubes using ionic wind from corona discharges, Exp. Fluids 40 (2006) 231

Weinberg, F.J., Carleton, F.B., Dunn-Rankin, D., Development of electrically charged extinguishant dispersions for use in microgravity, Combust. Sci. and Technol., 175:12 (2003) 2161

Yue, Y., Hou, J., Ai, Z., Yang, L., Zhang, Q., Experimental studies of the enhanced heat transfer from a heating vertical flat plate by ionic wind, Plasma Sci. Technol., Vol. 8, No.6, (2006) 697

Zhao, L., Adamiak, K., EHD Flow in Air Produced by Electric Corona Discharge in Pin-Plate Configuration, J. Electrostat. 63 (3-4) (2005) 337

Zhao, H., Liu, X., Tse, S.D., Control of Nanoparticle Size and Agglomeration through Electric-Field-Enhanced Flame Synthesis, J Nanopart Res (2008) 10:907-923